1 **Protein features for assembly of the RNA editing helicase 2 subcomplex**
2 **(REH2C) in Trypanosome holo-editosomes**

3

4 Vikas Kumar[1#], Pawan K. Doharey[1#], Shelly Gulati[2#], Joshua Meehan[1], Mary G. Martinez[1],
5 Karrisa Hughes[2], Blaine H.M. Mooers[2*] and Jorge Cruz-Reyes[1*]

6

7 [1] Department of Biochemistry and Biophysics, Texas A&M University, College Station, Texas,
8 United States of America.

9 [2] Department of Biochemistry & Molecular Biology, University of Oklahoma Health Sciences
10 Center, Oklahoma City, Oklahoma, United States of America.

11

12 * Corresponding author:

13 e-mail: cruzrey@tamu.edu

14 * Correspondence may also be addressed to:

15 e-mail: blaine-mooers@ouhsc.edu

16

17 # These authors contributed equally to this work.

18

19

Abstract

Uridylate insertion/deletion RNA editing in *Trypanosoma brucei* is a complex system that is not found in humans, so there is interest in targeting this system for drug development. This system uses hundreds of small non-coding guide RNAs (gRNAs) to modify the mitochondrial mRNA transcriptome. This process occurs in holo-editosomes that assemble several macromolecular *trans* factors around mRNA including the RNA-free RNA editing core complex (RECC) and auxiliary ribonucleoprotein (RNP) complexes. Yet, the regulatory mechanisms of editing remain obscure. The enzymatic accessory RNP complex, termed the REH2C, includes mRNA substrates and products, the multi-domain 240 kDa RNA Editing Helicase 2 (REH2) and an intriguing 8-zinc finger protein termed REH2-Associated Factor 1 (^{H2}F1). Both of these proteins are essential in editing. REH2 is a member of the DExH/RHA subfamily of RNA helicases with a conserved C-terminus that includes a regulatory OB-fold domain. In trypanosomes, ^{H2}F1 recruits REH2 to the editing apparatus, and ^{H2}F1 downregulation causes REH2 fragmentation. Our systematic mutagenesis dissected determinants in REH2 and ^{H2}F1 for the assembly of REH2C, the stability of REH2, and the RNA-mediated association of REH2C with other editing *trans* factors. We identified functional OB-fold amino acids in eukaryotic DExH/RHA helicases that are conserved in REH2 and that impact the assembly and interactions of REH2C. ^{H2}F1 upregulation stabilized REH2 *in vivo*. Mutation of the core cysteines or basic amino acids in individual zinc fingers affected the stabilizing property of ^{H2}F1 but not its interactions with other examined editing components. This result suggests that most, if not all, fingers may contribute to REH2 stabilization. Finally, a recombinant REH2 (240 kDa) established that the full-length protein is a *bona fide* RNA helicase with ATP-dependent unwinding activity. REH2 is the only DExH/RHA-type helicase in kinetoplastid holo-editosomes.

Introduction

Kinetoplastid protozoa including *Trypanosoma brucei* are early-branching eukaryotes that require extensive insertion and deletion of uridylates in most mitochondrial mRNAs (reviewed in 1). This RNA editing is protein-catalyzed and directed by small guide RNAs (gRNAs) with complementarity to fully-edited mRNA. Most editing progresses in blocks that typically overlap and each block is directed by a single gRNA (2). The editing machinery includes multiple subcomplexes: the ~20S catalytic RNA editing core complex (RECC, also called the 20S editosome) and auxiliary editing RNPs. The ~15S REH2-associated complex (REH2C) characterized here includes RNA editing helicase 2 (REH2), REH2-associated protein factor 1 (^{H2}F1), ^{H2}F2, and mRNA substrates and products (3, 4). However, only REH2 and ^{H2}F1 participate in editing. REH2C interacts with a larger accessory editing RNP complex termed the RNA editing substrate binding complex (RESC), which also contains mRNA (5, 6). The presence of mRNA in RESC was confirmed by others (7, 8).

RESC contains two modules that are intimately associated with each other: the gRNA-binding complex (GRBC) typified by the GAP1/GAP2 (alias GRBC2/GRBC1) heterotetramer that binds and stabilizes gRNA, and the more loosely defined RNA editing mediator complex (REMC) (6). REMC is typified by RGG2 and promotes editing progression (8-10). Other mRNA *trans* factors include a subcomplex containing MRB6070 and MRB1590, and RNA helicase REH1 that associate with holo-editosomes via stable or transient RNA contacts, respectively (11-13). The finding that the editing RNPs carry mRNA and gRNA implied that mRNA-gRNA hybrids form on multi-RNP platforms, and that transient addition of the RECC enzyme to the substrate-loaded platforms completes the assembly of the holo-editosome (3-8).

The editing apparatus is further complicated by the occurrence of variants of GRBC, REMC and RECC that may be regulatory (reviewed in 1) but the precise control mechanisms in editing remain unclear. However, the helicase REH2C subcomplex may play an important

71 regulatory role. REH2 is the largest characterized member of the DExH/RNA helicase A (RHA)
72 subfamily of proteins (14). These proteins are monomeric and contain a conserved C-terminal
73 domain cluster with a characteristic auxiliary oligonucleotide-binding (OB fold) domain (3, 14-
74 16). The OB fold in some RNA helicases is known to bind protein regulators or mediate RNA-
75 dependent activation of these enzymes (17). DExH/RHA proteins have a N-terminus with a
76 variable domain organization of less clear function. The N-terminal half of the REH2 carries two
77 predicted double-stranded RNA binding domains: dsRBD1 and dsRBD2 (14). Other
78 characterized DExH/RHA-type proteins that carry two N-terminal dsRBDs are the RNA helicase
79 RHA (aka DHX9) in vertebrates and its orthologous RNA helicase MLE (*maleless*) in flies (18).
80 Recombinant versions of the REH2 C-terminal half and full-size octa-zinc finger ^{H2}F1 formed a
81 stable complex *in vitro* (4). However, ^{H2}F1 is an unusual binding partner of DExH/RHA proteins
82 that typically associate with G-patch proteins (17). A genetic knockdown of ^{H2}F1 prevented
83 RNA-mediated association of REH2 with other editing components and caused fragmentation of
84 REH2 *in vivo*. Those results indicated that ^{H2}F1 is an adaptor protein and may stabilize REH2
85 (4).

86 The current study identified features in REH2 and ^{H2}F1 that affect the binding of these
87 proteins with each other, the stability of REH2, and RNA-mediated stable or transient
88 association of the REH2C subcomplex with other editing components *in vivo*. About 20 different
89 protein variants were examined *in vivo*. Comparisons of the REH2 with other eukaryotic
90 DExH/RHA helicases identified conserved OB fold residues that affect the assembly and
91 interactions of REH2C and are also important in distant processes, namely mRNA splicing in
92 yeast, and the assembly of the dosage compensation complex in fly. ^{H2}F1 upregulation
93 stabilized the large REH2 polypeptide *in vivo*. However, mutation of individual zinc fingers
94 compromised the stabilizing property of ^{H2}F1 but not its association with REH2 or other
95 examined components of the editing apparatus. Most if not all fingers may contribute to REH2

stabilization. Finally, we used a recombinant protein construct to establish that the isolated full-length REH2 (240 kDa) is a *bona fide* RNA helicase enzyme with ATP-dependent unwinding activity. REH2C is most likely an enzymatic editing RNP in kinetoplastid holo-editosomes.

Results

Previous studies revealed that the native REH2C exhibits RNA-mediated interactions with at least two variants of RESC (3-5). These variants contain gRNA and comparable levels of GAP1 and RGG2, that typify GRBC and REMC, respectively. However, these variants differ minimally in their relative content of the canonical MRB3010 in GRBC. Additional variations in protein composition have been reported in purifications of RESC components by different labs (reviewed in 1). Interestingly, native and genetically-induced changes in MRB3010 stoichiometry may be common. While the precise reasons for these changes are unclear, we reasoned that they reflect relevant dynamic changes in the assembly and function of the editing apparatus. In this study, we examined protein features that affect the formation of REH2C, its stable association with RESC components, and its transient contacts with the RECC enzyme. Because the examined helicase-associated RESC variant exhibits substoichiometric MRB3010, we refer to its variant GRBC module as GRBC* (4). Using antibodies made available to us, we have detected other proteins in pulldowns of REH2 that may be part of this RESC variant including both GAP1/GAP2 paralogs and MRB8170. The REH2 pulldowns also contain MRB6070 that was found in a MRB6070/MRB1590 subcomplex that associates via RNA with RESC (11)(S1 Fig.). However, further analysis of relative composition between variants is needed.

Analysis of REH2 mutants *in vivo*

121 We analyzed the importance of specific features of REH2, both in the formation of REH2C
122 and in the association of this subcomplex with other components in holo-editosomes (constructs
123 listed in Fig. 1A). To this end, we expressed a tetracycline (Tet)-inducible REH2 wild-type (WT)
124 construct with a Tandem Affinity Purification (TAP) tag (3) and examined its co-purification with
125 endogenous ^{H2}F1 and GAP1 proteins, of REH2C and GRBC, respectively. We found that ectopic
126 REH2 was able to reconstitute interactions of the native REH2 protein in trypanosomes (Fig. 1B-C,
127 lanes 1-2, respectively). With this system in hand, we tested the assembly of REH2 variants bearing
128 truncations or point mutations in an approach that has been used in other eukaryotic DExH/RHA
129 helicases (16, 19). All REH2 mutants examined were directly compared and normalized to a WT
130 construct used as control. Neither overexpression or depletion of REH2 affects the steady-state
131 level of its binding partner ^{H2}F1 or the examined GRBC proteins (3, 4).
132
133 **Fig. 1. *In vivo* analyses of REH2 variants. (A)** Scheme of REH2 WT (2167 residues) and
134 variants with the examined truncations or point mutations in the N- and C-terminal regions (NTR
135 and CTR). The mutations, affected domains, and predicted molecular weight of the constructs
136 are listed. Identified domains: dsRBD1 and dsRBD2 (double-stranded RNA binding domains 1
137 and 2), CORE (catalytic core RecA1 and RecA2 domains), HA2 (helicase associated helical
138 bundle domain), and OB (OB fold-like domain). **(B-C)** Western blots of IgG pulldowns from
139 extracts to examine the association of tagged REH2 WT or deletion mutants with endogenous
140 ^{H2}F1 and GAP1 (in GRBC*). An uninduced (-Tet) control lane is included. The data are
141 representative of at least three biological replicates for each mutant. A few non-specific species
142 cross-react with the antibodies in some assays. The position of IgG is marked. Sizing markers
143 (M) are in kDa. **(D)** Charts of the relative level of ^{H2}F1 and GAP1 in the pulldowns.
144 Representative assays from panels A-B and other pulldowns in this study were used to plot +/-1
145 SD, *n*=3 for each mutant. The ^{H2}F1/REH2 and GAP1/REH2 ratios in each REH2 mutant were
146 normalized to the ratios in REH2 WT (= 1, in the plot). Assays with signals that were too low

147 were not determined (n.d.). REH2 was often fragmented, so only the full-length polypeptide was
148 scored. Some deletion mutants were present at higher level than tagged REH2 WT in the
149 induced extracts.
150
151 *N- and C-truncations*. We examined N- and C-terminal regions (NTR and CTR) flanking the
152 catalytic and helicase associated domains RecA1/RecA2 and HA2, respectively, in REH2. We
153 removed sequences in the unique NTR (>1000 residues) in the REH2 variants ∆N and ∆Nds. Next,
154 we removed the CTR after the OB fold (123 residues) or from the OB fold (260 residues) in the ∆AOB
155 and ∆OB variants, respectively. REH2 and its orthologs in kinetoplastids carry the longest N terminus
156 in the known DExH/RHA-type helicases (~1300 residues in REH2 from *T. brucei*) (14). Direct
157 comparisons with the REH2 WT construct showed that the examined N- and C-resections reduced
158 the association of the shortened REH2 polypeptides with ^{H2}F1 and GAP1 proteins (Figs. 1B-D). This
159 suggested that both termini of REH2 may contribute to the normal assembly of REH2C and its RNA-
160 mediated interactions with other editing components *in vivo*. The dsRBDs, the OB fold, and
161 undefined features in the N and C termini may be involved. It is also conceivable that the examined
162 sequence resections may impact the global conformation of REH2, thereby indirectly affecting its
163 protein interactions. In that case, the normal REH2 interactions in the editing apparatus may be
164 sensitive to overall changes in the integrity or conformation of REH2. A comparison of REH2 ∆N and
165 ∆Nds in whole-cell and enriched-mitochondrial extracts indicated that these large truncations do not
166 prevent mitochondrial import (S2 Fig). Because the CTR includes a potentially regulatory OB fold in
167 DExH/RHA-type RNA helicases (16), we focused on this domain in the subsequent studies of REH2.
168
169 *Point mutations*. Our structural searches of the OB fold-like domain in REH2 using Phyre2
170 (20) found the best agreements of the REH2 OB fold with structures of yeast ADP-bound Prp43p
171 helicase and *Drosophila* RNA helicase MLE in a complex with RNA and ADP-Alf4 (4, 16, 18, 21).

172 Prp43p is a bi-functional helicase in mRNA splicing and ribosome biogenesis (15, 22). The helicase
173 MLE remodels roX RNA substrates to promote assembly of the dosage compensation complex in
174 *Drosophila* (18). We examined specific residues in the predicted OB fold of REH2 that seem to be
175 conserved in the DExH/RHA helicases mentioned above (Fig. 2 A-D). OB point mutations were
176 compared to two controls: REH2 WT and a mutation in dsRBD2 (dsR) that reduces the association of
177 REH2 with GAP1, gRNA and mRNA (Fig. 2A, lanes 1 and 2, respectively) (3). The β1−β2 and β4−β5
178 loops in the OB fold may include determinants in nucleic acid recognition (Fig. 2D) (16, 18). In
179 helicase Prp43p, mutation of K704 (β4−β5 loop), which is exposed to the solvent in the Prp43p
180 structure, decreased the RNA affinity and ATPase activity of the helicase *in vitro* (16). Sequence
181 alignments and a homology model derived from the structure of Prp43p matched K704 in Prp43p
182 with R2023 in the predicted β4−β5 loop in REH2 (S3 Fig)(4). We also examined R1979 in REH2 that
183 is not conserved in Prp43p and may serve as an internal control. Pulldowns of the R1979A and
184 R2023A mutants suggest that neither mutation alters the association of REH2 with ^{H2}F1 (Figs. 2A-C).
185 R1979A did not appear to affect the REH2 association with GAP1. However, R2023A caused a
186 moderate decrease in the association with GAP1, implying that at least R2023A could be disruptive
187 in trypanosomes.

188 In helicase MLE, several residues in the OB fold bind to specific uridylates in U-rich
189 sequences in roX transcripts. Mutation of some of these residues impaired RNA binding by MLE *in*
190 *vitro* or the proper localization of MLE in chromosomes (18). Sequence alignments and homology
191 models indicated that the residues H1032 and K1033 in MLE likely represent residues H1998 and
192 R1999 in the predicted β3−β4 loop in the OB fold in REH2 (Fig. 2D; S4 Fig)(21). The H1998E mutant
193 appeared to retain a normal association with ^{H2}F1 but exhibited a moderate decrease in association
194 with GAP1. In contrast, R1999E either alone or together with H1998E (98/99) exhibited a more
195 robust decrease (over 60%) in association with both ^{H2}F1 and GAP1 (Fig. 2A-C). This indicated that
196 H1998 and R1999 contribute to the assembly of the REH2 helicase with other editing components.

197 However, R1999 has a higher impact on such interactions than the adjoining H1998. As expected,
198 the dsR mutant used as a control exhibited a strong decrease in association with GAP1. However,
199 the dsR mutation did not seem to affect the association of REH2 with ^{H2}F1 (Figs. 2A, 2C). Pulldowns
200 of the mutants were normalized to the REH2 WT control as in Fig. 1.
201
202 **Fig. 2. *In vivo* analyses of REH2 variants.** Western blots of IgG pulldowns as in Fig. 1 to
203 examine the association of endogenous ^{H2}F1 and GAP1 (in GRBC*) with tagged REH2 WT or
204 variants with point mutations at: **(A)** the OB fold domain including R1979A (1979), H1998E
205 (1998) and R1999E (1999). The previously characterized dsR mutant with an inactivating
206 double mutation in the dsRBD2 was included for comparison (3). A few non-specific species
207 crossreact with the antibodies in some assays; and **(B)** the OB fold domain including double
208 1998/1999 (98/99) or single R2023A (2023) mutations. **(C)** Charts of the relative levels of ^{H2}F1
209 and GAP1 in the pulldowns. Assays from panels A-B and biological replicate pulldowns in this
210 study were used to plot +/-1 SD, *n*=2 or *n*=3 for each mutant. The ^{H2}F1/REH2 and GAP1/REH2
211 ratios in each REH2 mutant were normalized to the ratios in REH2 WT (= 1, in the plot). **(D)**
212 Secondary structure prediction of the OB fold with α-helix (cylinders) and β-strand (arrows)
213 elements, and the position of point mutations examined indicated by arrows.
214
215 Table 1 summarizes observed effects of the examined mutations in REH2 on its association
216 with ^{H2}F1 and GAP1. While large protein truncations in REH2 may alter the global conformation of
217 the polypeptide, relevant point mutations in REH2 are more likely to cause specific functional effects.
218 Our systematic mutagenesis of REH2 suggests an intricate interaction network including features
219 across both N- and C- terminal regions of REH2 that affect the assembly of REH2C, and the
220 association of this subcomplex with GAP1-associated RNPs *in vivo*. Remarkably, these observations
221 also indicate that equivalent residues in the auxiliary conserved OB fold domain in DExH/RHA

222 helicases function in disparate RNA processes in the taxonomically distant species of trypanosomes,
223 yeast, and fly.

224 **Table 1. Association of REH2 constructs with ^{H2}F1 and GAP1**

REH2-TAP variant	Association in pulldown		Reference
	^{H2}F1	GAP1	Construct described
WT	control*	control*	23
ΔN	decreased	decreased	This study
ΔNds	decreased	decreased	This study
ΔOB	decreased	decreased	This study
ΔAOB	decreased	decreased	This study
dsR	control-like †	decreased	3
1979	control-like	control-like	This study
1998	control-like	decreased	This study
1999	decreased	decreased	This study
98/99	decreased	decreased	This study
2023	control-like	decreased	This study

* The WT construct served as positive control to assess relative association of mutant constructs.
225 † Comparable to the level observed with the WT construct.
226

227 ## Analysis of ^{H2}F1 mutants *in vivo*
228
229 To analyze specific features of the ^{H2}F1 zinc finger protein in trypanosomes, we expressed a
230 Tet-inducible TAP tagged ^{H2}F1 WT construct and examined its association with endogenous REH2,
231 GAP1 and REL1 proteins. REL1 is a subunit of the editing enzyme RECC. We found that the tagged
232 ^{H2}F1 WT was able to reconstitute interactions of the native ^{H2}F1 protein in trypanosomes (Fig. 3).
233 Notably, expression of the ectopic ^{H2}F1 WT increased the steady-state level of endogenous REH2
234 compared to a control lane without tetracycline (Fig. 3A, lanes 1-2; Fig. 3B). As a control to mark the
235 position of REH2 we used a reported RNAi-based knockdown of ^{H2}F1 that decreases the level of
236 endogenous REH2 (Fig. 3A, lanes 5-7; Fig. 3B)(4). The contrasting effects of the upregulation and
237 downregulation of ^{H2}F1 on the endogenous REH2 are consistent with the idea that ^{H2}F1 stabilizes
238 REH2 *in vivo*. We examined the distribution of REH2 and ^{H2}F1, and canonical proteins in RESC and
239 RECC, in sedimentation analyses of mitochondrial extract (S5 Fig). REH2 is heterodispersed as
240 shown before (23) and overlaps with ^{H2}F1 in the gradient. However, the relative abundance of these

241 proteins at high and low densities differs substantially. It is possible that the association between
242 REH2 and ^{H2}F1 or their stoichiometry in REH2C varies *in vivo*. Additional studies will be necessary to
243 examine these possibilities.
244
245 **Fig 3. Effect of expressing ^{H2}F1 WT or Znf5 C2>A2 on the REH2 steady-state abundance.**
246 **(A)** Western blots of extracts with tagged ^{H2}F1 WT (lanes 1-2) or Z5 C2>A2 (Z5; lanes 3-4).
247 Control assays include lanes without Tet-induction. Control lanes with a reported ^{H2}F1-RNAi
248 construct mark the position of the endogenous REH2 and ^{H2}F1. The RNAi lanes show the
249 induced decrease of ^{H2}F1 and concurrent fragmentation of REH2 full-length. Hash marks
250 indicate full-length and two prominent fragments of REH2 (4). GAP1 was used as a loading
251 control in all assays in this panel. Molecular size markers (M). A typical C2H2 zinc finger domain
252 fold is depicted with core cysteine substitutions C2>A2 (arrows), other conserved residues, and
253 variable residues (black circles). **(B)** Charts of the relative levels of endogenous REH2 full-
254 length in the extracts +/-1 SD, *n*=3. Induced/uninduced ratios of REH2 for each construct were
255 further normalized to GAP1. **(C-D)** Western blots of IgG pulldowns of WT and Z5 constructs
256 showing association with endogenous REH2, GAP1, REL1, and endogenous ^{H2}F1. REL1 is
257 examined by radiolabeled self-adenylation. Other proteins are examined as in panel A. Non-
258 specific species (*) may represent fragments of the tagged protein that react with the antibodies.
259 **(E)** Charts of the relative levels of REH2, GAP1 and REL1 in the pulldowns +/-1 SD, *n*=3. The
260 ratios (protein/tagged-bait) in the Z5 mutant were normalized to ratios in the ^{H2}F1 WT construct.
261
262 To determine if the stabilizing effect of ^{H2}F1 requires one or more zinc finger (Znf) domains,
263 we introduced amino acid substitutions that either disrupt the canonical fold of the domain (by
264 replacing the canonical residues) or eliminate the positive charge (by replacing various basic
265 residues with neutral residues) in individual fingers of the ectopic construct. The examined ^{H2}F1
266 mutants are summarized in Table 2. The location of the fingers and the examined substitutions

267 (including between 2 and 6 basic residues per finger) in the full sequence of ^{H2}F1 are shown in S6
268 Fig. All ^{H2}F1 mutants examined were directly compared and normalized to a WT construct used
269 as control in all panels. This enabled the separation of mutants in multiple panels.

270 **Table 2. ^{H2}F1 mutants with reduced ability to stabilize REH2 *in vivo***

^{H2}F1-TAP variant	Endogenous REH2 *Steady-state level*	Figures using this construct
WT	**Increased***	Figs. 3, 4 and 5
Znf5 C2>A2	no change †	Fig. 3
Znf1 R/K>A	no change	Fig. 4
Znf2 R/K>A	no change	Fig. 4
Znf3 R/K>A	no change	Fig. 4
Znf4 R/K>A	no change	Fig. 5
Znf5 R/K>A	no change	Fig. 4
ΔN	no change	Fig. 5
ΔC	no change	Fig. 5

* ^{H2}F1-WT ectopic expression increased the level of endogenous REH2
271 † No change (i.e., level within stardard deviation for at least two biological replicates)
272
273 *Canonical cysteine residues*. We changed two cysteines to two alanines (C2>A2) to disrupt
274 the native conformation of the predicted zinc fingers (Fig. 3A). We began by disrupting Znf5 because
275 of its significant homology to a reported dsRNA-bound C2H2 zinc finger domain structure (4, 14, 24).
276 Mutants are referred to in the text by the acronym in the general form Znf*X*. A shorter version of the
277 acronym is used in the figure annotations. The resulting mutant protein Znf5 C2>A2 did not induce an
278 evident increase in the steady-state level of endogenous REH2 as we found after expressing the
279 ^{H2}F1 WT construct. This was evident in direct comparisons of extracts that contain similar levels of
280 ectopic ^{H2}F1 protein, WT or Znf5 C2>A2 (Fig. 3A, lanes 1-4; Fig. 3B). To examine whether the lack of
281 Znf5 affected the association of ^{H2}F1 with other editing components, we performed IgG pulldown
282 assays of tagged ^{H2}F1. These assays showed that the ^{H2}F1 WT and Znf5 C2>A2 variants similarly
283 associated with endogenous helicase REH2, GAP1 and REL1 ligase (Figs. 3C, 3E). Notably,
284 pulldowns of both tagged ^{H2}F1 WT and Znf5 C2>A2, contain endogenous ^{H2}F1 (Fig. 3D). The above
285 data suggest that Znf5 is not essential for the normal association of ^{H2}F1 with other editing

286 components. We cannot rule out that the endogenous ^{H2}F1 is “saving” the examined associations
287 with the mutant ^{H2}F1.
288 We also attempted to generate a ^{H2}F1 variant bearing a triple C2>A2 substitution in Znf6,
289 Znf7 and Znf8. However, expression of this construct was unstable and eventually lost in culture.
290 Together, the observations above suggest that ^{H2}F1 may require a full complement of zinc fingers in
291 their native conformation to stabilize REH2 but not to associate with the examined editing
292 components.
293
294 *Variable basic residues*. Because the native conformation of the zinc fingers seems required
295 for ^{H2}F1 to stabilize REH2 we introduced mutations that decrease the positive charge in the zinc
296 fingers yet likely to retain native conformation (25). We expressed ^{H2}F1 variants to test the role of
297 several basic residues around the core residues that are mostly located between the second cysteine
298 and the first histidine (Fig. 4A) (26). Specifically, we introduced R/K>A substitutions (between 2 and 6
299 per finger) to decrease the positive charge in the zinc fingers and to remove potential charge-charge
300 interactions with REH2 or associated RNAs. As above, we use in the text the acronym in the general
301 form Znf*X* but a shorter version of the acronym in the figures. Our functional analyses of Znf1, Znf2,
302 Znf3 or Znf5 R/K>A variants showed that the loss of positive charge in any of these zinc fingers
303 reduced the ability of ^{H2}F1 to induce the accumulation of intact endogenous REH2 in extracts (Figs.
304 4B-C). However, these mutations did not prevent the association of ^{H2}F1 with REH2, GAP1 and
305 REL1 (Figs. 4D-F). These expressed ^{H2}F1 variants also co-purified with endogenous ^{H2}F1 at a level
306 comparable to the WT construct (Figs. 4D, 4F). The data above indicated that the wildtype and
307 R/K>A variant proteins associated similarly with the examined editing components. Overall, ^{H2}F1 may
308 require that most zinc fingers retain their native conformation and positive charge to efficiently
309 increase the stability of REH2. However, the loss of the native conformation or positive charge in
310 individual fingers does not preclude the assembly of ^{H2}F1 in the REH2C, or the association of this
311 subcomplex with the examined editing components. Detection of endogenous ^{H2}F1 in our pulldowns

312 suggest the presence of ^{H2}F1 multimers. Pulldowns treated with an RNaseA/T1 mixture suggest that
313 the association between tagged ^{H2}F1 and endogenous ^{H2}F1 is RNase-resistant (S7 Fig.). We note the
314 possibility that the tested ^{H2}F1 mutants may exhibit defects in the examined associations and that
315 these defects are masked by the endogenous ^{H2}F1. However, the reduced stabilizing property of the
316 mutants was not saved by the endogenous ^{H2}F1. Further studies using isolated recombinant proteins
317 are needed to establish direct protein contacts between ^{H2}F1 monomers as was shown between
318 REH2 and ^{H2}F1 (4).
319
320 **Fig. 4. *In vivo* analyses of ^{H2}F1 variants with reduced positive charge in Znf1, Znf2, Znf3**
321 **or Znf5 (variable residues R/K>A).** Figure annotations use a shorter acronym of each mutant
322 in the form: Z*X,* as in Fig. 3. **(A)** Cartoon of ^{H2}F1 (524 residues). Multi-sequence alignment of
323 the eight C2H2 zinc fingers, indicating the core cysteines and histidines (boxes) and R/K>A
324 substitutions of variable residues (between 2 and 6) in each finger (open circles). The C2H2
325 zinc finger domain fold is depicted as in Fig. 3. In this case, the arrows illustrate three variable
326 residue substitutions R/K>A. **(B)** Western blots of extracts as in Fig. 3A of induced tagged ^{H2}F1
327 WT and Z1, Z2, Z3 and Z5 R/K>A mutants or uninduced control. GAP1 was used as a loading
328 control (lanes 1-7). **(C)** Chart of steady-state level of endogenous REH2 full-length in extracts
329 with each construct as in Fig. 3B. **(D-E)** Western blots and self-adenylation reactions of IgG
330 pulldowns of ^{H2}F1 WT and Z1, Z2, Z3 and Z5 R/K>A mutants showing association with
331 endogenous REH2, ^{H2}F1, REL1 and GAP1. Non-specific species in pulldowns (*) are indicated.
332 (**F)** Charts of the relative level of associated endogenous proteins in the pulldowns +/-1 SD, *n=2*
333 or *n*=3, as in Fig. 3. The ratios (protein/tagged-bait) in the mutants were normalized to ratios in
334 the ^{H2}F1 WT construct.
335
336 *N- and C-truncations*. Because mutagenesis of the tested Znf domains did not prevent the
337 association of ^{H2}F1 with other editing components *in vivo*, we asked if fragments of ^{H2}F1 retain these

338 interactions. To test this question, we expressed N- or C-terminal fragments including Znf1-to-Znf3
339 (termed ΔC) or Znf4-to-Znf8 (termed ΔN) that span 49% and 51% of the ^{H2}F1 polypeptide chain,
340 respectively (Fig. 5A, bottom). These two fragments exhibited minimal or no association with the
341 examined endogenous REH2, ^{H2}F1, or REL1 ligase (Figs. 5A). These mutants were directly
342 compared with the ^{H2}F1 WT and Znf4 R/K>A constructs. We note that while Znf4 R/K>A was
343 examined separately from the R/K>A variants in Fig. 4, all R/K>A mutants are normalized to the ^{H2}F1
344 WT construct and uniduced lane that were included in each gel. As with other R/K>A mutants,
345 Znf4 R/K>A did not cause an evident increase in the steady-state level of endogenous REH2 in
346 extracts as we found with the ^{H2}F1 WT construct. The relative level of endogenous REH2 was 1.0 +/-
347 10% in the induced extract with Znf R/K>A normalized to the uninduced control. The Znf4 R/K>A and
348 other Znf R/K>A mutations in the current study retained all tested interactions that are observed with
349 the ^{H2}F1 WT control. However, the ΔN and ΔC constructs failed to establish basic interactions with
350 the tested editing components. Because the native REH2C subcomplex carries mRNA (4), we
351 wondered if the ^{H2}F1 ΔN and ΔC constructs also fail to co-purify with mRNA. To this end, we
352 quantitated the relative content of mitochondrial transcripts in the pulldowns of the WT, ΔN, and ΔC
353 constructs in biological replicate experiments that were performed in triplicate (Fig. 5B). The
354 examined mitochondrial transcripts include examples of unedited, edited, and never-edited mRNA
355 (ND4), and ribosomal RNA 9S. We also examined cytosolic transcripts (Tubulin, 1400 and 1390) to
356 score non-specific RNA interactions of editing subcomplexes as in previous pulldown studies (5).
357 Relative to the ^{H2}F1 WT control used for normalization, both ΔN and ΔC pulldowns exhibited a
358 dramatic loss in bound mitochondrial mRNAs (Fig. 5B, upper and middle panels). Interestingly, the
359 level of cytosolic mRNAs was similar in the ΔN and WT proteins but dramatically less in the ΔC
360 variant. The latter variant lost most examined RNA interactions: specific and non-specific. An
361 exception may be mitochondrial RNA 9S. We also compared the relative impact of the ΔN and ΔC
362 deletions with a more discrete alteration in Znf4 R/K>A (Fig. 5B, lower panel). The level of

363 mitochondrial RNAs in the Znf4 pulldown was similar to that of the ^{H2}F1 WT control. However, the
364 level of cytosolic transcripts decreased ~70 fold in Znf4 R/K>A. The independent pulldowns and RNA
365 quantitation in three equivalent experiments showed consistent results in the protein interactions and
366 RNA content of these ^{H2}F1 constructs. The above data indicated that the tested ^{H2}F1 fragments
367 appear to have lost the normal direct interaction of ^{H2}F1 WT with REH2 in REH2C, and the normal
368 RNA-dependent association of ^{H2}F1 WT with other examined proteins in the editing apparatus.
369 Quantitation of the examined transcripts in the input extracts (including those used in the pulldowns
370 in Figs. 5A-B) confirmed that the observed dramatic loss in RNA association with ΔN and ΔC
371 constructs was not due to large changes in the transcript level at steady state (S8 Fig.). The ^{H2}F1 ΔN
372 construct used a heterologous mitochondrial leader sequence (see methods and S1 Table). A
373 comparison of ^{H2}F1 ΔN and ΔC in whole-cell and enriched-mitochondrial extracts suggest that ^{H2}F1
374 ΔN localizes to mitochondria efficiently. However, the import or retention of ^{H2}F1 ΔC into mitochondria
375 is relatively compromised. At least some import of the ^{H2}F1 ΔC construct may occur in comparison
376 with a control cytosolic marker in whole-cell and enriched-mitochondrial extracts (S2 Fig.). Apparent
377 fragmentation of ^{H2}F1 ΔC (TAP tag panel in S2 Fig.) suggests that this construct is also partially
378 unstable. These results indicate that features in the N terminus of ^{H2}F1 are required for efficient ^{H2}F1
379 association with mitochondrial editing proteins and transcripts in the pulldowns. The C-terminal
380 truncation affected the ^{H2}F1 association with all examined transcripts (including cytosolic) and
381 somehow also its mitochondrial import and stability. The expressed ^{H2}F1 ΔC construct may not
382 entirely reflect the ability of the N-terminal half of ^{H2}F1 to bind editing proteins and transcripts due to
383 the reduced localization and stability of this construct. Finally, the more discrete alteration in Znf4
384 R/K>A may have caused a relatively mild decrease in RNA affinity that mostly affected weak, non-
385 specific interactions, e.g., by cytosolic RNA in the pulldowns of ^{H2}F1.
386
387 **Figure 5. *In vivo* analyses of ^{H2}F1 terminal deletion and Znf4 R/K>A mutants. (A)** Western

388 blots of IgG pulldowns of N and C truncation mutants (ΔN and ΔC) that removed fingers 1-to-3
389 and fingers 4-to-8, respectively, and the Z4 R/K>A variant. Association of the constructs with
390 endogenous REH2, ^{H2}F1 and REL1 was examined. Biological replicates of these assays
391 suggest a similar quality and loading of samples in the pulldowns. Cartoon of ^{H2}F1 with zinc
392 fingers and a line marking the N and C truncations. Non-specific species in pulldowns (*) are
393 indicated. **(B)** qRT-PCR quantitation of transcripts in the pulldowns in panel A. dCq of IgG
394 pulldowns of tagged protein (induced extract) normalized to a mock pulldown (uninduced
395 extract) [dCq = $2^{(\text{test Cq} - \text{mock Cq})}$] for each construct. The mutant proteins were then normalized to
396 the tagged WT protein. All values took into account the recovery of tagged protein in each
397 pulldown in panel A. Three independent biological replicates with Cq average values and one
398 standard deviation (+/-1 SD, *n*=3) were plotted. Non-specifically associated cytosolic transcripts
399 differed substantially in pulldowns of different mutants, so these transcripts were not used as
400 reference. Mitochondrial unedited (UE) and edited (ED) and cytosolic RNA transcripts are
401 indicated. RPS, Murf, and 9S are abbreviations for RPS12, Murf2, and 9S rRNA, respectively.
402 1390 and 1400 are abbreviations for the cytosolic HGPRT isoforms Tb927.10.1390 and
403 Tb927.10.1400, respectively. Tub is tubulin. Other short names are standard.
404

405 **Analysis of recombinant REH2 *in vitro***
406
407 The conserved predicted catalytic domains in REH2, the unwinding activity in pulldowns of
408 REH2 or ^{H2}F1 from extracts, and the loss of this activity in the pulldowns after mutating catalytic
409 amino acids in REH2, indicate that REH2 in the context of its native subcomplex functions as an RNA
410 helicase (3, 4, 23). However, the unwinding activity of the isolated REH2 has not been formally
411 established. We have now generated a his-tagged recombinant full-length rREH2 polypeptide (240
412 kDa) without its mitochondrial leader sequence (see the methods section) that supports robust ATP-
413 dependent unwinding of a synthetic dsRNA substrate *in vitro.* This polypeptide is largely intact in

414 most preparations (Fig. 6A). The dsRNA substrate in our assay is a mimic of the native A6 editing
415 system formed by pre-annealing of a 3' fragment of the pre-mRNA A6 with a cognate gRNA.
416 The synthetic A6 mRNA/gRNA pair supports a full round of U-deletion editing in an *in vitro*
417 assay with cell extracts and purified RECC enzyme (27, 28). The unwinding activity of the
418 recombinant enzyme increased in a titration with increasing concentrations of rREH2, and also in a
419 time course up to 30 min when most of the annealed radiolabeled RNA was unwound (Figs. 6B-C).
420 An upshift of radiolabeled RNA in a ribonucleoprotein complex (RNP) at the highest tested
421 concentrations of rREH2 (12 pmoles) in the titration (Fig. 6B) may be due to the known RNA binding
422 activity of the native REH2 established by UV crosslinking (5, 23). The radiolabeled strand (gRNA)
423 alone or in heat-treated controls of the dsRNA substrate exhibit the same gel mobility as the
424 helicase-unwound gRNA (Figs. 6C-D). In summary, the isolated 240 kDa recombinant REH2 is a
425 *bona fide* RNA helicase enzyme *in vitro*, and further supports the idea that REH2 may remodel RNA
426 or its RNPs in editing.
427
428 **Figure 6. Recombinant rREH2 is a catalytically active RNA helicase. (A)** Purified rREH2[30-
429 2167] samples in a denaturing gel stained with Coomassie. NTA-Ni elution fractions 1-to-3 are
430 shown with molecular size markers (kDa). **(B)** Unwinding assays in 10 μL reaction mixtures with
431 increasing concentrations of rREH2[30-2167] +/- ATP. An RNP complex (RNP) forms at the
432 highest enzyme concentration tested; **(C)** Unwinding assays at increasing incubation times with
433 rREH2[30-2167] +/- ATP using the standard reaction mixture described in the material and
434 methods section. The standard reaction used a molar excess of enzyme over substrate. The
435 dsRNA (ds) was assembled by pre-annealing of synthetic transcript that mimics a 3' fragment of
436 the *T. brucei* A6 pre-edited mRNA and a radiolabeled cognate guide RNA (27). Radiolabeled
437 unwound ssRNA (ss) is indicated. Input dsRNA was heat denatured (Δ) as control. The assays in
438 this panel were treated with proteinase K to remove any RNP that may accumulate (see methods).

439 **(D)** Additional controls showing that the starting radiolabeled ssRNA used to generate the
440 dsRNA substrate in the assay and the unwound radiolabeled ssRNA in the heat-denatured (Δ)
441 dsRNA (in panel C) have the same gel mobility.
442

443 Discussion

444
445 In the current study, we examined over 20 constructs of REH2 and ^{H2}F1 (Tables 1 and 2) to
446 identify features in these editing proteins that impact the stability of REH2, the assembly of the
447 REH2C RNP, and its RNA-mediated coupling with other components of the RNA editing holoenzyme
448 (or RNA holo-editosome). We also formally established that the isolated REH2 is a *bona fide* RNA
449 helicase enzyme.
450
451 The mRNA editing *trans* factors core enzyme RECC and accessory RESC and REH2C
452 exhibit transient and stable contacts with each other via RNA. Variants of RECC and the RESC
453 modules, GRBC and REMC, are also emerging in studies by different labs (reviewed in 1). These
454 variants imply a dynamic nature of holo-editosomes that may be important in editing control and
455 needs further characterization. The helicase complex REH2C exhibits transient and stable contacts
456 with variants of RESC that minimally differ in the relative content of MRB3010 (in the GRBC module).
457 This study focused on stable interactions by REH2C that can be readily examined. Prior studies *in*
458 *vivo* showed that inactivating mutations in the helicase ATP binding site or the dsRBD2 domain
459 dissociate REH2 from mRNA and RESC components, suggesting a general helicase detachment
460 from the editing apparatus (3). ^{H2}F1 RNAi dissociates the helicase from canonical proteins in the
461 RESC modules. RNAi knockdown of either ^{H2}F1 or REH2 also inhibited the editing associated with a
462 RESC variant that is particularly active and transiently interacts with REH2C (3, 4). These and other

463 observations indicate that transient and stable contacts in dynamic holo-editosomes including
464 those involving REH2C are important.
465 A systematic mutagenesis in the current study identified features affecting the assembly of
466 the REH2C RNP, or its association with other editing components *in vivo.*
467

468 **REH2 mutants *in vivo***
469
470 The NTR truncations examined here (>1000 residues each), ΔN and ΔNds, caused a major
471 loss in ^{H2}F1 binding and RNA-mediated association with GAP1. The only difference between the ΔN
472 and ΔNds constructs is that the latter lacks the ~70 amino acid dsRBD2 domain. As mentioned
473 above, the dsRBD2 promotes the addition of REH2 into holo-editosomes (3). Also, the dsRBD2 in the
474 related helicase MLE in flies may provide a major RNA-binding surface (29, 30). The tested
475 truncations suggest that other N-terminal features besides dsRBD2 may contribute to normal
476 interactions by REH2 *in vivo*. These truncations may also introduce topological changes that alter the
477 normal REH2 interactions but do not prevent localization of the constructs in enriched-mitochondrial
478 extracts (S2 Fig.). Conformational changes were proposed to modulate interactions by other
479 eukayotic DExH/RHA helicases (18, 31). Overall, the tested NTR truncations may indicate the
480 presence of unidentified protein features or global changes in conformation that affect the REH2
481 interactions. Further studies will be needed to resolve these possibilities. However, relatively short
482 CTR truncations and point mutations that affected the REH2 interactions with other editing
483 components are less likely to cause major conformation changes in REH2.
484
485 We have speculated that the conserved OB fold in DExH/RHA subfamily helicases may
486 share functional residues in kinetoplastid RNA editing and other RNA processes (14). Our examined
487 C-terminal truncations included most of the CTR (260 residues in ΔOB) or elements beyond the
488 OB fold that may be specific of REH2 (123 residues in ΔAOB). We examined R2023 in REH2

489 that corresponds to R704 in helicase Prp43p in yeast spliceosomes (16) (S3 Fig.). R2023
490 should be located in a critical loop, β4-β5, in the REH2 OB fold. In yeast, R704 is poised to
491 interact with the RNA substrate entering the helicase cavity, and mutation of this residue inhibits
492 the RNA binding and RNA-mediated activation of Prp43p (16). We also examined R1979 in
493 REH2, which is not conserved in Prp43p. In trypanosomes, the R2023A substitution had a
494 moderate effect on the stable RNA-mediated association of REH2C with GAP1. However,
495 R1979A did not evidently affect this interaction. Neither R1979A or R2023A seem to
496 significantly affect the REH2 direct interaction with ^{H2}F1.
497 Similarly, H1998 and R1999 in REH2 were compared to the equivalent H1032 and
498 K1033 positions in the RNA helicase MLE in flies. The later residues in MLE bind specific
499 uridylates in U-rich roX boxes of the cognate roX RNA. H1032 and K1033 are also needed for
500 the chromosomal localization of MLE in the *Drosophila* dosage compensation complex (18). The
501 H1998E substitution had a moderate effect on the REH2 association with GAP1 but had little or
502 no effect on the interaction with ^{H2}F1. In contrast, the adjacent substitution R1999E affected
503 both the direct REH2 interaction with ^{H2}F1 and the RNA-based REH2 association with GAP1.
504 These results are consistent with the idea that ^{H2}F1 is an adaptor protein of REH2 (4), and that
505 structure-function correlations may be traceable to specific conserved amino acids in REH2 and
506 related helicases in highly-diverged species (14). This is also in line with the idea that the OB
507 fold in DExH/RHA helicases, including REH2, is a conserved regulatory domain.
508

509 **^{H2}F1 mutants *in vivo***
510
511 ^{H2}F1 has eight predicted C2H2 Znf domains that cover over ~45% of the polypeptide
512 sequence. Apart from the Znf domains, ^{H2}F1 has no evident sequence or structural conservation
513 outside of the kinetoplastids. ^{H2}F1 is an adaptor protein that brings the REH2 to the editing machinery
514 (4) and it also stabilizes REH2. That is, the induced downregulation of ^{H2}F1 caused fragmentation of

515 REH2 (4), and we showed here that the converse upregulation of ^{H2}F1 increased the REH2 level *in*
516 *vivo*. ^{H2}F1 may require most of its zinc fingers to stabilize REH2 because loss of the core structure or
517 positive charge in individual fingers compromised this function. It is feasible that the stabilizing effect
518 of ^{H2}F1 involves substantial changes in the helicase conformation and coordination of its zinc fingers.
519 Notably, all examined ^{H2}F1 substitution-mutants were able to associate with REH2, GAP1, and REL1.
520 This suggested that the basic fold or positive charge of the fingers is not essential for the ^{H2}F1
521 association with other editing components. However, N- or C-terminal truncation of nearly half the
522 size of ^{H2}F1 hampered its normal interactions with the examined editing components. The ^{H2}F1 ΔN
523 accumulated in enriched-mitochondrial extracts but the ^{H2}F1 ΔC localization in mitochondria seemed
524 relatively compromised. Somehow the C-terminal truncation was particularly deleterious to ^{H2}F1.
525 Additional studies are needed to pinpoint specific determinants for ^{H2}F1 direct binding to REH2 or its
526 RNA-mediated contacts with other components.

527 Besides the REH2•^{H2}F1 system, other DExH/RHA helicase•Znf protein pairs have been
528 characterized (14). In the DXH30•ZAP system in antivirus protection in humans, the antiviral protein
529 ZAP has four Znf motifs that participate in viral RNA recognition (32, 33). All four fingers lie on a
530 positively charged surface in a crystal structure of ZAP (25) and mutation of basic residues in the
531 fingers inhibited the ZAP antiviral function (33). The ZAP studies imply that stabilization of REH2 by
532 ^{H2}F1 could involve a precise topology of its zinc fingers, and that the ^{H2}F1 fingers may participate in
533 RNA binding. Notably, recombinant ZAP is multimeric (25). If ^{H2}F1 dimerizes, a single REH2C RNP
534 would include 16 zinc fingers. The co-purification of tagged and endogenous ^{H2}F1 from RNase-
535 treated extracts imply direct protein contacts between the ^{H2}F1 copies (S7 Fig.). However, analyses
536 of recombinant ^{H2}F1 WT and mutants are necessary to establish the potential of ^{H2}F1 to multimerize
537 and bind RNA, and to define the role of its fingers. The RNA content in pulldowns of the ^{H2}F1 Znf4
538 variant with four R/K>A substitutions suggested minimal changes in association with target RNAs in
539 mitochondria but a significance loss in non-specific contacts with unrelated transcripts. This suggests

540 that subtle changes in RNA affinity are more likely to affect weak non-specific RNA contacts. The
541 general loss of transcripts examined in the pulldowns of the tested ^{H2}F1 fragments also suggests that
542 efficient RNA association by the REH2C complex *in vivo* involves at least the majority of zinc fingers
543 in ^{H2}F1. We note that the transcripts examined may associate with either ^{H2}F1, REH2 or both proteins
544 in the native REH2C RNP.
545

546 REH2 may function as an RNA helicase in kinetoplastid RNA editing
547
548 Prior studies suggested that REH2 is a functional helicase in RNA editing. REH2 pulldowns
549 from GAP1-depleted extracts exhibit RNA unwinding activity (4), and the mutation of catalytic
550 residues in the predicted RecA1 domain inhibits the unwinding activity in pulldowns of REH2 (23).
551 We have now established that the isolated full-length recombinant REH2 (240 kda) is a *bona fide*
552 RNA helicase enzyme. This further indicates that REH2, the only DExH/RHA helicase in kinetoplastid
553 holo-editosomes provides an ATP-dependent unwinding activity in RNA editing. Additional studies
554 are needed to determine if ^{H2}F1 affects the activity of REH2. Besides REH2, the editing apparatus
555 also requires the DEAD-box RNA helicase REH1 (12, 13). REH1 is not part of the RNPs studied here
556 and seems to lack a direct binding partner. A transient RNA-mediated interaction of REH1 with
557 other editing proteins has been detected (23, 34). REH1 and REH2 are functionally different.
558 REH2 is needed for editing within single blocks, including the first “initiating” block (3). In
559 contrast, REH1 is needed for editing of two or more blocks (i.e., by overlapping gRNAs) but has
560 no effect on the first block, suggesting a role in gRNA exchange (13). Both RNA helicases may
561 promote critical remodeling of RNA or RNP structure. Our ongoing RNA-seq analyses may
562 provide additional functional insights concerning REH2C (Kumar et al., unpublished).
563

564 Possible roles of editing complex variants
565
566 The editing apparatus much like the splicing and transcription molecular machines may

567 exhibit dynamic phases of assembly and function. The RECC enzyme has multiple isoforms that
568 include several RNase III (RIII)-like protein subunits. These RIII proteins have the potential to
569 form a large number of binary combinations that could modulate substrate recognition (35-37).
570 Also, natural GRBC and REMC isoforms and genetically-induced changes in their protein/RNA
571 organization are emerging. A recurring theme is the variable interaction between the essential
572 GAP1/2 heterotetramer and MRB3010 (GRBC6) (1, 6, 38) that is potentially regulatory. For
573 example, GRBC variants in pulldowns of MRB3010 or REH2 differ in relative content of
574 MRB3010 and editing level in associated mRNAs (3, 5). Also, RNAi of REH2 or ^{H2}F1 caused a
575 reduced editing in mRNAs in the MRB3010 pulldowns (3, 4). REH2 and ^{H2}F1 features, including
576 those examined here, may affect specific steps in the editing mechanism and we are currently
577 addressing this.
578

579 # Materials and Methods
580

581 ## Cell Culture
582

583 *T. brucei* Lister strain 427 29-13 procyclic was grown axenically in log phase in SDM79
584 medium (39) and harvested at a cell density of 1–3x10^7 cells/mL. All transgenic cell lines were
585 induced with tetracycline at 1µg/mL. The REH2 WT-TAP and ^{H2}F1 RNAi cell lines that were
586 used as controls were generated in our lab (3, 4). We have seen that the TAP tag in REH2,
587 including the WT construct, seems to slow the growth of trypanosomes after several days of
588 culture (23). This and presumably incomplete cloning after transfection may account for the
589 uneven expression levels in extracts from independent subcultures. To partially control for this
590 issue, most plasmid constructs used to generate the current data figures were made to use
591 puromycin selection. Most transfections used tetracycline-screened HyClone Fetal Bovine
592 Serum (FBS) (SH30070.03T; GE Healthcare). This enabled a faster cell recovery after
593 transfection than with constructs using phleomycin selection that were originally used in cell

594 lines and appeared somewhat less stable during subculture. Regardless of this issue,
595 independent analyses of protein associations were consistent with either puromycin or
596 phleomycin constructs.
597

598 **DNA Constructs**
599
600 All overexpression and RNAi studies used inducible plasmid constructs. The constructs
601 for ^{H2}F1 RNAi and the REH2 dsRBD2 mutant K1078A/A1086D were previously reported (3, 4).
602 N-terminal deletion constructs for REH2 (ΔN and ΔNds) and ^{H2}F1 (ΔN) were prepared using the
603 In-Fusion® HD Cloning Kit (639648; Clontech). Two PCR amplicons were prepared in each
604 case using CloneAmp™ HiFi PCR Premix (638500; Clontech) and were then gel-eluted using
605 NucleoSpin® Gel and PCR Clean-up (740609.10; Clontech). One amplicon encodes the first 34
606 amino acids of REH2 (primers: F-1503, R-1522), including the predicted REH2 mitochondrial
607 leader sequence (REH2-MLS) (23), that was used for all N-deletion constructs. The other
608 amplicon included the remaining relevant gene fragment sequence: 3070-6501 bases (REH2
609 ΔN), 3280-6501 bases (REH2 ΔNds), or 766-1572 bases (^{H2}F1 ΔN). Three-piece in-fusion
610 reactions were performed to join the two amplicons and pLEW79-ada-TAP plasmid linearized at
611 *XhoI* and *BamHI* (40). The PCR primers (S1 Table) included 5' and 3' terminal homology (15
612 bases) to enable the recombination-based fusion between the amplicons and the plasmid DNA.
613 The REH2 (ΔAOB and ΔOB) and ^{H2}F1 ΔC deletion constructs are also recombination-based
614 fusions of the amplified relevant gene fragment with linearized plasmid DNA. The REH2
615 constructs R2023A, H1998E, R1999E and H1998E/R1999E, and the ^{H2}F1 construct Znf5
616 2C>2A were created by site-directed mutagenesis in inverse-PCR reactions of the pLEW79-
617 ada-TAP WT plasmid as the template. pLEW79-ada-TAP was modified from the original
618 pLEW79-TAP (40, 41). The resulting linearized mutant constructs were circularized using the In-
619 Fusion HD Cloning Kit. Other ^{H2}F1 constructs used synthetic gBlock gene fragments (IDT) with

620 mutations. N-terminal fragments of ^{H2}F1 (Znf1, Znf2 and Znf3 R/K>A single finger mutants)
621 replaced the corresponding sequence in the ^{H2}F1 WT construct after digestion with *XhoI* and the
622 internal *ApaI* site in ^{H2}F1. A C-terminal fragment of ^{H2}F1 to generate Znf4R/K>A or Znf5 R/K>A
623 replaced a corresponding sequence in the ^{H2}F1 WT construct after digestion with *ApaI* and
624 *BamH1*. The ^{H2}F1 WT construct was made by ligation of an amplicon with the full open reading
625 frame into pLEW79-ada-TAP plasmid linearized at *XhoI* and *BamHI.* All constructs were
626 confirmed by DNA sequencing, linearized with *NotI*, and transfected in trypanosomes (39).
627

628 **Western Blots**
629
630 Western blots of REH2, ^{H2}F1 and ^{H2}F2 (subunits of REH2C), GAP1 (alias GRBC2;
631 subunit of GRBC) and A2 (alias MP42; subunit of RECC) were performed as reported (4, 23).
632 Western blots of the GAP1/GAP2 (alias GRBC2/GRBC1) paralogs simultaneously, and of
633 MRB8170 and MRB6070 (subunits of REMC and MRB6070/1590 assemblies, respectively),
634 were performed as previously described (42, 43). GAP1 alone was examined in the main data
635 figures. Both GAP1/GAP2 were examined in S1 and S5 figures. Peroxidase Anti-peroxidase
636 antibody (P1291; Sigma) diluted to 1:200 (v/v) was used to detect the TAP-tag. EF-1 α1
637 antibody (sc-21758; Santa Cruz Biot) diluted to 1:200 (v/v) was used as a cytosolic marker.
638 Protein quantitative analyses using Amersham ECL™ western blot detection reagents were
639 performed in an Amersham Imager 600.
640

641 **Radioactivity Assays**

642

643 RNA ligases in the RECC enzyme were radiolabeled by self-adenylation directly on the
644 beads in IgG pulldowns (44). Unwinding assays of REH2 used reported conditions with a few
645 modifications (4) and full-length recombinant His-REH2. The dsRNA substrate in these assays

646 used an A6 mRNA/gRNA pair (23). The A6 pair mimics the endogenous ATPase subunit 6
647 substrate. The gRNA was transcribed with RNA T7 polymerase from an amplicon (S1 Table)
648 after *DraI* restriction digestion and gel purification of the product. The 61-nt gRNA was 5'-
649 labelled with γ^{32}P-ATP using T4 Polynucleotide kinase. The 62-nt mRNA was synthetic (IDT). A
650 mix with 3 pmoles of labelled gRNA and 12 pmoles of mRNA was heated at 95° C for 3 min,
651 and then immediately incubated for 30 min at room temperature in the annealing buffer (10 mM
652 MOPS pH 6.5, 1 mM EDTA, and 50 mM KCl). The annealed RNA hybrids were isolated from
653 native 12% PAGE run at 4 ˚C at 50 V for 120 min in 0.5x Tris-borate-EDTA buffer. Standard 10
654 μL reaction mixtures in unwinding buffer (40 mM Tris-Cl pH 8.0, 0.5 mM $MgCl^2$, 0.01% Nonidet
655 P-40, and 2 mM DTT) were incubated for 30 min at 19 °C with 20 cps of hybrid (~20 fmoles)
656 and 3 µg of recombinant REH2 (~12 pmoles). Variations to the standard assay including in the
657 concentration of REH2 or the reaction time are indicated in the text. All assays contained 100
658 fmoles of unlabeled gRNA as competitor to prevent re-annealing of unwound γ^{32}P-gRNA. The
659 assays were stopped with an equal volume of 2x helicase reaction stop buffer (50 mM EDTA,
660 1% SDS, 0.1% bromophenol blue, 0.1% xylene cyanol, and 20% glycerol) and kept on ice for 5
661 min. The assays in Fig. 6C were also treated with 0.4U of proteinase K (P8107S; NEB), 25 mM
662 EDTA and 0.5% SDS at 22° C for 30 min. The entire reaction was loaded onto a native 12%
663 PAGE and resolved at 25 V for 120 min at 4°C.
664

665 **Cell Extracts and Purification of Protein and RNA from IgG Pulldowns**
666
667 Whole cell extracts as well as mitochondria-enriched (mini-mito) extracts were used in
668 this study. Whole-cell extracts were generated by incubation of cell pellets in MRB-Triton buffer
669 (25 mM Tris-Cl pH 8.0, 10 mM MgOAC, 1 mM EDTA, 10 mM KCl, 5% glycerol, 0.5% Triton X-
670 100) at 4 °C for 45 minutes followed by centrifugation at 15,000g for 30 minutes. Mitochondria-
671 enriched extracts were prepared using a simplified protocol similar to others reported earlier (2,

672 45). Namely, cell pellets were resuspended into hypotonic DTE buffer (1 mM Tris-HCl pH 8.0, 1
673 mM EDTA pH 8.0) supplemented with protease inhibitors and disrupted in a Dounce
674 homogenizer. The suspension was passed through a 26-gauge needle as originally described
675 (46). The enriched mitochondrial vesicles were spun down and the cytosolic content in the
676 supernatant discarded. This step improved the recovery of intact REH2 compared to whole-cell
677 extracts. REH2 is more prone to fragmentation than other proteins examined in this study. The
678 following steps were also as in (46). The pellet was resuspended into STM buffer (0.25M
679 Sucrose, 20 mM Tris-HCl pH 8.0, 2 mM $MgCl_2$) supplemented with DNase I, RNase-free
680 (EN0523; Fisher Scientific). The reaction was stopped with one volume of STE buffer (0.25 M
681 Sucrose, 20 mM Tris-HCl pH 8.0, 2 mM EDTA pH 8.0). The enriched mitochondria were spun
682 down and washed in STE buffer. The pellet was resuspended into MRB-Triton buffer and
683 incubated in ice for 15 min. The suspension was spun down at 15,000g at 4 °C for 30 min. The
684 supernatant was collected and stored at -80 °C. In IgG pulldowns of the extracts, ectopically
685 expressed TAP-REH2 and TAP-^{H2}F1 were recovered as reported (4, 23) with some
686 modifications. Approximately 2 mg of protein was mixed with 1x SUPERase·In™ RNase
687 inhibitor (Invitrogen™) and incubated with Dynabeads IgG (11203D; Invitrogen™). The beads
688 were washed five times with 1ml of wash buffer (150 mM NaCl, 1 mM EDTA, 10 mM MgAOc,
689 0.1% NP-40, and 25 mM Tris pH 8.0). Protein was eluted from the beads with 15 μL of 1x SDS
690 loading buffer at 95 °C for 2 min. RNA was extracted by treating the beads with 4U proteinase K
691 (NEB) for 2 hrs at 55 °C, followed by phenol extraction and ethanol precipitation. For some
692 pulldowns, RNase A/T1 mix (EN0551; Fisher Scientific) was applied at 20 U/mg of protein both
693 in the input extract and again while bound to the beads.
694

695 **Quantitative RT-PCR**
696

697 Isolated RNA from the pulldowns or directly from input extracts was treated with DNase
698 I, RNase-free (EN0523; Thermo Scientific™) prior to cDNA synthesis with the iScript™ Reverse
699 Transcription Supermix (Bio-Rad) as described elsewhere (5). The amplifications mixtures (10
700 µl) used SsoAdvanced™ Universal SYBR® Green Supermix (Bio-Rad) and reported
701 oligonucleotides for unedited mRNAs, fully edited mRNA, and reference transcripts (47). Diluted
702 samples of the examined cDNA produced a single amplicon during linear amplification under
703 our conditions. The end-point amplicons described here have been gel-isolated, cloned and
704 confirmed by sequencing as previously described (5). Fold-enrichment of mitochondrial and
705 cytosolic transcripts in IgG pulldowns of tagged proteins (induced extracts), relative to a mock
706 pulldown (uninduced extract), was calculated as follows: Fold = $2^{[-ddCq]}$, where ddCq = Cq test
707 IP – Cq mock IP, as in (5). The relative value for each mutant construct was adjusted to the
708 amount of recovered tagged protein, and subsequently normalized to the tagged WT construct
709 (= 1). The plot in Fig. 5B was constructed using data from 3 independent biological replicate
710 experiments, including a total of six amplicons per data point (i.e., two technical replicate
711 amplicons per assay). Two of the independent experiments (including cultures +/- Tet for each
712 mutant) were performed concurrently. The third independent experiment (one set of cultures per
713 mutant +/- Tet) was conducted on a subsequent date. The replicate experiments showed a
714 consistent sample loading in the assays used in our plots. The examined mutant constructs
715 differed in the amount of non-specific association with Tubulin and other cytosolic transcripts
716 that are normally used as internal reference in antibody pulldowns using a common protein bait.
717 The raw Cq values of examined editing transcripts in the pulldowns and the plotted values after
718 normalization indicated a substantial loss of these transcripts in the truncated mutants.
719 qRT-PCR assays of input extract in S8 Fig. were normalized using the following equation: Ratio
720 (reference/target) = $2^{[Cq(ref) - Cq(target)]}$. This scores the relative difference between the reference
721 and target Cq values. The current plots of input extract used 18S rRNA as reference (S8 Fig.).

722 We obtained similar results with any of these cytosolic transcripts used as a reference: tubulin,
723 1400 or 1390 (Tb927.10.1400 or Tb927.10.1390, respectively).
724

725 Homology Modeling and Bioinformatics Analysis

726
727 The multiple-sequence alignment of REH2 and MLE, and that of the ^{H2}F1 zinc finger
728 domains, was done with Clustal Omega (48). Formatting of the fingers alignment was done with
729 BOXSHADE version 3.21 (http:/www.ch.embnet.org/software/BOX_form.html). Sequence
730 alignment of Prp43p, REH2, and other helicases was done using the CDD tool in NCBI (49).
731 The structure-based searches of *T. brucei* REH2 used the program Phyre2 (20). The homology
732 model of REH2 derived from the structure of yeast Prp43p. The inset is a closer view of R2023
733 and the surround region in the OB-fold. The molecular surface is colored by
734 residue conservation. The image was made using PyMOL version 2.2.
735

736 Recombinant Protein

737
738 6xHis-REH2 (amino acid residues 30-2167) was amplified by PCR (S1 Table). The gel-
739 purified product was cloned into the NcoI and BamHI sites in the expression vector pET15b by
740 using the NEBuilder® HiFi DNA Assembly Master Mix (E262, NEB) and the appropriate primers.
741 The ligation reaction mixtures were transformed into chemically competent Omnimax cells from
742 ThermoFisher Scientific. Colonies with the correct insert were identified by single-colony PCR
743 and then amplified for plasmid purification. The sequence of the flanking vector region and the
744 insert was checked by DNA sequencing. The plasmid DNA was transformed into Rosetta2 DE3
745 cells (Novagen Inc.) and overexpressed in 4 L of Terrific Broth media by supplementing 2% (v/v)
746 ethanol and 2 mM $MgCl_2$ at 37 °C. Protein induction with 0.5 mM IPTG was done at a OD_{600} of
747 0.8, and the expression was continued for 22 hours at 16 °C. The cell pellet was stored at -80
748 °C overnight and was resuspended in lysis buffer (5 mL/g of cell pellet) of 50 mM Tris-HCl pH
749 8.0, 250 mM NaCl, 1 mM EDTA, and 1 mM DTT along with 10 µg of RNase-free DNase and 15

750 mg of hen egg white lysozyme. The cells were lysed in an Emulsiflex hydraulic press. The cell
751 debris was pelleted at 39,200 x g for 30 minutes at 4 °C. The supernatant with 6xHis-REH2 was
752 batch attached to equilibrated Qiagen Ni-NTA Agarose at 4 °C for 16 hrs. The helicase was
753 eluted with 50 mM Tris-HCl pH 8.0, 300 mM NaCl, 1 mM DDT, and 250 mM imidazole. The first
754 elution of the purification was dialyzed into unwinding assay buffer. This material was tested for
755 the presence of the recombinant protein in 6% SDS-PAGE stained with Commassie blue,
756 western blots and antibody pulldowns, and for activity in dsRNA unwinding activity assays *in*
757 *vitro*.
758

759 # Acknowledgements
760

761 We thank the Read lab for their gift of antibodies against GAP1, TbRGG2 (alias RGG2),
762 MRB6070, MRB8170, and ^{H2}F2. The Afasizhev lab kindly provided antibodies that react against
763 the GAP1/GAP2 paralogs (alias GRBC2/GRBC1) simultaneously. We also thank the Stuart lab
764 for providing the antibodies against A2 (alias MP42). Amna Mushtaq provided detailed
765 comments on the manuscript. Jana Gomez, Elizabeth Alvarez and Melissa Yang helped with
766 the preparation of figures.
767

768 # References
769

770 1. Cruz-Reyes J, Mooers BHM, Doharey PK, Meehan J, Gulati S. Dynamic RNA
771 holoeditosomes with subcomplex variants: Insights into the control of trypanosome editing.
772 WIREs RNA. 2018;e1502.
773 2. Koslowsky DJ, Sun Y, Hindenach J, Theisen T, Lucas J. The insect-phase gRNA
774 transcriptome in Trypanosoma brucei. Nucleic acids research. 2013.
775 3. Madina BR, Kumar V, Mooers BH, Cruz-Reyes J. Native Variants of the MRB1 Complex
776 Exhibit Specialized Functions in Kinetoplastid RNA Editing. PloS one. 2015;10(4):e0123441.
777 4. Kumar V, Madina BR, Gulati S, Vashisht AA, Kanyumbu C, Pieters B, et al. REH2C
778 Helicase and GRBC Subcomplexes May Base Pair through mRNA and Small Guide RNA in
779 Kinetoplastid Editosomes. J Biol Chem. 2016;291(11):5753-64.

780 5. Madina BR, Kumar V, Metz R, Mooers BH, Bundschuh R, Cruz-Reyes J. Native
781 mitochondrial RNA-binding complexes in kinetoplastid RNA editing differ in guide RNA
782 composition. RNA. 2014;20(7):1142-52.
783 6. Aphasizheva I, Zhang L, Wang X, Kaake RM, Huang L, Monti S, et al. RNA binding and
784 core complexes constitute the U-insertion/deletion editosome. Mol Cell Biol. 2014;34(23):4329-
785 42.
786 7. Huang Z, Faktorova D, Krizova A, Kafkova L, Read LK, Lukes J, et al. Integrity of the
787 core mitochondrial RNA-binding complex 1 is vital for trypanosome RNA editing. RNA. 2015.
788 8. McAdams NM, Simpson RM, Chen R, Sun Y, Read LK. MRB7260 is essential for
789 productive protein-RNA interactions within the RNA editing substrate binding complex during
790 trypanosome RNA editing. RNA. 2018;24(4):540-56.
791 9. Simpson RM, Bruno AE, Bard JE, Buck MJ, Read LK. High-throughput sequencing of
792 partially edited trypanosome mRNAs reveals barriers to editing progression and evidence for
793 alternative editing. RNA. 2016;22(5):677-95.
794 10. Simpson RM, Bruno AE, Chen R, Lott K, Tylec BL, Bard JE, et al. Trypanosome RNA
795 Editing Mediator Complex proteins have distinct functions in gRNA utilization. Nucleic acids
796 research. 2017;45(13):7965-83.
797 11. Shaw PL, McAdams NM, Hast MA, Ammerman ML, Read LK, Schumacher MA.
798 Structures of the T. brucei kRNA editing factor MRB1590 reveal unique RNA-binding pore motif
799 contained within an ABC-ATPase fold. Nucleic acids research. 2015;43(14):7096-109.
800 12. Missel A, Souza AE, Norskau G, Goringer HU. Disruption of a gene encoding a novel
801 mitochondrial DEAD-box protein in Trypanosoma brucei affects edited mRNAs. Mol Cell Biol.
802 1997;17(9):4895-903.
803 13. Li F, Herrera J, Zhou S, Maslov DA, Simpson L. Trypanosome REH1 is an RNA helicase
804 involved with the 3'-5' polarity of multiple gRNA-guided uridine insertion/deletion RNA editing.
805 Proc Natl Acad Sci U S A. 2011;108(9):3542-7.
806 14. Cruz-Reyes J, Mooers BH, Abu-Adas Z, Kumar V, Gulati S. DEAH-RHA helicase•Znf
807 cofactor systems in kinetoplastid RNA editing and evolutionarily distant RNA processes. RNA
808 Dis. 2016;3(2):e1336.
809 15. Jarmoskaite I, Russell R. RNA helicase proteins as chaperones and remodelers. Annu
810 Rev Biochem. 2014;83:697-725.
811 16. Walbott H, Mouffok S, Capeyrou R, Lebaron S, Humbert O, van Tilbeurgh H, et al.
812 Prp43p contains a processive helicase structural architecture with a specific regulatory domain.
813 EMBO J. 2010;29(13):2194-204.
814 17. Robert-Paganin J, Rety S, Leulliot N. Regulation of DEAH/RHA helicases by G-patch
815 proteins. Biomed Res Int. 2015;2015:931857.
816 18. Prabu JR, Muller M, Thomae AW, Schussler S, Bonneau F, Becker PB, et al. Structure
817 of the RNA Helicase MLE Reveals the Molecular Mechanisms for Uridine Specificity and RNA-
818 ATP Coupling. Mol Cell. 2015;60(3):487-99.
819 19. Dhote V, Sweeney TR, Kim N, Hellen CU, Pestova TV. Roles of individual domains in
820 the function of DHX29, an essential factor required for translation of structured mammalian
821 mRNAs. Proc Natl Acad Sci U S A. 2012;109(46):E3150-9.
822 20. Kelley LA, Mezulis S, Yates CM, Wass MN, Sternberg MJ. The Phyre2 web portal for
823 protein modeling, prediction and analysis. Nat Protoc. 2015;10(6):845-58.
824 21. Cruz-Reyes J. MBHM, Kumar K., Doharey P.K., Meehan J., Chaparro L. Control
825 Mechanisms of the Holo-Editosome in Trypanosomes. In: J C-R, M G, editors. RNA Metabolism
826 in Mitochondria. Nucleic Acids and Molecular Biology. 34: Springer, Cham; 2018.
827 22. Jankowsky E. RNA helicases at work: binding and rearranging. Trends in biochemical
828 sciences. 2011;36(1):19-29.

829 23. Hernandez A, Madina BR, Ro K, Wohlschlegel JA, Willard B, Kinter MT, et al. REH2
830 RNA helicase in kinetoplastid mitochondria: ribonucleoprotein complexes and essential motifs
831 for unwinding and guide RNA (gRNA) binding. J Biol Chem. 2010;285(2):1220-8.
832 24. Segal DJ, Crotty JW, Bhakta MS, Barbas CF, 3rd, Horton NC. Structure of Aart, a
833 designed six-finger zinc finger peptide, bound to DNA. J Mol Biol. 2006;363(2):405-21.
834 25. Chen S, Xu Y, Zhang K, Wang X, Sun J, Gao G, et al. Structure of N-terminal domain of
835 ZAP indicates how a zinc-finger protein recognizes complex RNA. Nat Struct Mol Biol.
836 2012;19(4):430-5.
837 26. Klug A. The discovery of zinc fingers and their development for practical applications in
838 gene regulation and genome manipulation. Q Rev Biophys. 2010;43(1):1-21.
839 27. Seiwert SD, Heidmann S, Stuart K. Direct visualization of uridylate deletion in vitro
840 suggests a mechanism for kinetoplastid RNA editing. Cell. 1996;84(6):831-41.
841 28. Rusche LN, Cruz-Reyes J, Piller KJ, Sollner-Webb B. Purification of a functional
842 enzymatic editing complex from Trypanosoma brucei mitochondria. EMBO J. 1997;16(13):4069-
843 81.
844 29. Izzo A, Regnard C, Morales V, Kremmer E, Becker PB. Structure-function analysis of the
845 RNA helicase maleless. Nucleic acids research. 2008;36(3):950-62.
846 30. Masliah G, Barraud P, Allain FH. RNA recognition by double-stranded RNA binding
847 domains: a matter of shape and sequence. Cell Mol Life Sci. 2013;70(11):1875-95.
848 31. Christian H, Hofele RV, Urlaub H, Ficner R. Insights into the activation of the helicase
849 Prp43 by biochemical studies and structural mass spectrometry. Nucleic acids research.
850 2014;42(2):1162-79.
851 32. Ye P, Liu S, Zhu Y, Chen G, Gao G. DEXH-Box protein DHX30 is required for optimal
852 function of the zinc-finger antiviral protein. Protein & cell. 2010;1(10):956-64.
853 33. Guo X, Carroll JW, Macdonald MR, Goff SP, Gao G. The zinc finger antiviral protein
854 directly binds to specific viral mRNAs through the CCCH zinc finger motifs. J Virol.
855 2004;78(23):12781-7.
856 34. Kruse E, Voigt C, Leeder WM, Goringer HU. RNA helicases involved in U-
857 insertion/deletion-type RNA editing. Biochimica et biophysica acta. 2013;1829(8):835-41.
858 35. Carnes J, Soares CZ, Wickham C, Stuart K. Endonuclease associations with three
859 distinct editosomes in Trypanosoma brucei. J Biol Chem. 2011;286(22):19320-30.
860 36. McDermott SM, Luo J, Carnes J, Ranish JA, Stuart K. The Architecture of Trypanosoma
861 brucei editosomes. Proc Natl Acad Sci U S A. 2016;113(42):E6476-E85.
862 37. Carnes J, McDermott S, Anupama A, Oliver BG, Sather DN, Stuart K. In vivo cleavage
863 specificity of Trypanosoma brucei editosome endonucleases. Nucleic acids research.
864 2017;45(8):4667-86.
865 38. Ammerman ML, Hashimi H, Novotna L, Cicova Z, McEvoy SM, Lukes J, et al. MRB3010
866 is a core component of the MRB1 complex that facilitates an early step of the kinetoplastid RNA
867 editing process. RNA. 2011;17(5):865-77.
868 39. Wirtz E, Leal S, Ochatt C, Cross GA. A tightly regulated inducible expression system for
869 conditional gene knock-outs and dominant-negative genetics in Trypanosoma brucei. Molecular
870 and biochemical parasitology. 1999;99(1):89-101.
871 40. Hernandez A, Panigrahi A, Cifuentes-Rojas C, Sacharidou A, Stuart K, Cruz-Reyes J.
872 Determinants for association and guide RNA-directed endonuclease cleavage by purified RNA
873 editing complexes from Trypanosoma brucei. J Mol Biol. 2008;381(1):35-48.
874 41. Panigrahi AK, Schnaufer A, Ernst NL, Wang B, Carmean N, Salavati R, et al.
875 Identification of novel components of Trypanosoma brucei editosomes. RNA. 2003;9(4):484-92.
876 42. Ammerman ML, Downey KM, Hashimi H, Fisk JC, Tomasello DL, Faktorova D, et al.
877 Architecture of the trypanosome RNA editing accessory complex, MRB1. Nucleic acids
878 research. 2012;40(12):5637-50.

879 43. Weng J, Aphasizheva I, Etheridge RD, Huang L, Wang X, Falick AM, et al. Guide RNA-
880 binding complex from mitochondria of trypanosomatids. Mol Cell. 2008;32(2):198-209.
881 44. Sabatini R, Hajduk SL. RNA ligase and its involvement in guide RNA/mRNA chimera
882 formation. Evidence for a cleavage-ligation mechanism of Trypanosoma brucei mRNA editing. J
883 Biol Chem. 1995;270(13):7233-40.
884 45. Hashimi H, Zikova A, Panigrahi AK, Stuart KD, Lukes J. TbRGG1, an essential protein
885 involved in kinetoplastid RNA metabolism that is associated with a novel multiprotein complex.
886 RNA. 2008;14(5):970-80.
887 46. Harris ME, Hajduk SL. Kinetoplastid RNA editing: in vitro formation of cytochrome b
888 gRNA-mRNA chimeras from synthetic substrate RNAs. Cell. 1992;68(6):1091-9.
889 47. Carnes J, Stuart KD. Uridine insertion/deletion editing activities. Methods in enzymology.
890 2007;424:25-54.
891 48. Sievers F, Higgins DG. Clustal Omega, accurate alignment of very large numbers of
892 sequences. Methods Mol Biol. 2014;1079:105-16.
893 49. Marchler-Bauer A, Derbyshire MK, Gonzales NR, Lu S, Chitsaz F, Geer LY, et al. CDD:
894 NCBI's conserved domain database. Nucleic acids research. 2015;43(Database issue):D222-6.
895

896

897 Supporting information

898

899 **S1 Figure. Western blot analyses of RESC associated proteins in antibody pulldowns of**

900 **REH2 and MRB3010**. Immunoprecipitations (IP) from extract with specific antibodies against

901 REH2, MRB3010 or CoxI (mock). **(A)** Western blot analyses examined for the presence of

902 REH2, MRB8170 and MRB6070 proteins. These are markers of REH2C, REMC and a

903 MRB6070/MRB1590-containing subcomplex that associates with RESC, respectively. Extract

904 (Ext) used in the IPs and size markers in kDa (M) are indicated. **(B)** Western blot analyses as in

905 A examining REH2, the GAP1/GAP2 paralogs, and MRB6070. We note that proteins in the IPs

906 are often upshifted relative to the control extract lane. The cause of this upshift is unclear to us

907 but it may be a slight effect on the proteins migration due to the presence of IgG in those

908 samples. IgG in the pulldown lanes is indicated.

909

910 **S2 Figure. Ectopically-expressed TAP constructs in whole-cell and enriched-**

911 **mitochondrial extracts**. Western blots of large-truncation constructs in whole-cell (WC) and

912 enriched-mitochondrial (aka Mini-Mito “MM” extract): (A) REH2-ΔN, (B) REH2-ΔNds, (C) ^{H2}F1-

913 ΔN, and (D) ^{H2}F1-ΔC. Western blots of the tag in these constructs (TAP), the cytosolic marker
914 eEF-1 (all panels), and endogenous REH2 (panels C and D) indicate a partial enrichment of the
915 REH2 deletion constructs in the mini-mito extract. Some mitochondrial enrichment of ^{H2}F1-ΔC is
916 apparent relative to eEF-1 but the localization of ^{H2}F1-ΔC is clearly compromised compared to
917 other constructs examined.
918
919 **S3 Figure. The OB-fold in yeast helicase Prp43p (crystal structure pdb: 2XAU_B) and *T.*
920 *brucei* REH2**. (A) Sequence alignment of Prp43p, REH2, and other DExH/RHA helicases. The
921 sequences were aligned using the CDD tool in NCBI. The residue R1979 in REH2 is not
922 conserved in the aligned sequences but the basic amino acid at position 2023 in REH2 (K704 in
923 Prp43p) is conserved. Secondary structure elements are indicated: α-helix (cylinders) and β-
924 strand (arrows). (B) homology model of R2023 in REH2 using the OB fold in Prp43p as a
925 template.
926
927 **S4 Figure. Multi-sequence alignment of a C-terminal segment in *T. brucei* REH2 and**
928 ***Drosophila* MLE DExH/RHA RNA helicases**. The alignment was generated with Clustal
929 Omega (48). Boxes were inserted manually to improve the match between the MLE and REH2
930 residues. Note that H1032, K1033 and T1034 (in red), which make U-specific contacts in MLE,
931 are aligned with H1998, R1999 and T2000 (in red) in REH2. Predicted α-helix (cylinders) and β-
932 strand (arrows) in REH2 are indicated.
933
934 **S5 Figure. Sedimentation analysis of endogenous editing proteins. (A)** 10-30% glycerol
935 gradients of freshly-made mitochondria-enriched extract from 29:13 procyclic trypanosomes.
936 Catalase and RECC complex were used as 11 S and 20 S markers, respectively (23).
937 Endogenous REH2, ^{H2}F1 and ^{H2}F2, GAP1 (GRBC2), GAP2 (GRBC1), and A2 (MP42) were
938 examined in western blots. All panels in this figure derived from the same extract fractions. The

939 data shown is representative of at least two panels for each protein in biological replicate
940 gradients.
941
942 **S6 Figure. Location of the zinc-finger substitutions examined in this study. (A)** Full ^{H2}F1
943 amino acid sequence including the location of eight C2H2 zinc-finger motifs (Znf1-to-8
944 highlighted in different colors)**. (B)** Zinc-finger motifs starting with the N terminal finger at the
945 top, and the amino acid positions spanning each finger in panel A. The R/K>A substitutions in
946 each finger that were examined in this study are marked by a dot.
947
948 **S7 Figure. RNase-resistant co-purification of tagged-^{H2}F1 and endogenous ^{H2}F1.** Western
949 blots of IgG pulldowns from extracts with or without an RNaseA/T1 mix. All panels in this figure
950 derive from the same blot. The upper blot with the tagged-^{H2}F1 bait was cut below the 75 kDa
951 marker. The middle and lower panels were divided between the 50 kDa and 37 kDa marker.
952 The 34.4 kDa RGG2, a typical subunit of the REMC module in the RESC complex. As expected,
953 the RNA-mediated association of RGG2 decreased with the RNase treatment.
954
955 **S8 Figure. Quantitation of steady-state RNA transcripts in the input mitochondrial**
956 **extracts used in the IgG pulldowns.** Independent biological replicates (two independent
957 cultures used in Fig. 5) with Cq average values and one standard deviation (+/-1SD, *n*=2) were
958 plotted. dCq of steady-state RNA transcripts in lysates relative to background 18s rRNA used as
959 reference [dCq = $2^{(\text{target Cq} - \text{ref Cq})}$]. Shorter bars indicate a smaller differential versus 18s rRNA in
960 the sample. For example, ND7 is relatively abundant compared to other transcripts in the
961 sample (i.e., it has a lower Cq). The WT construct is induced or not (+/-). All mutants are
962 induced. All end-point amplicons were examined in gels to confirm that they were single
963 products during linear amplification. Abbreviation of the RNA names is as in Fig. 5B.

964

965 **S1 Table. DNA oligonucleotides, gBlocks (IDT) and synthetic RNA.**

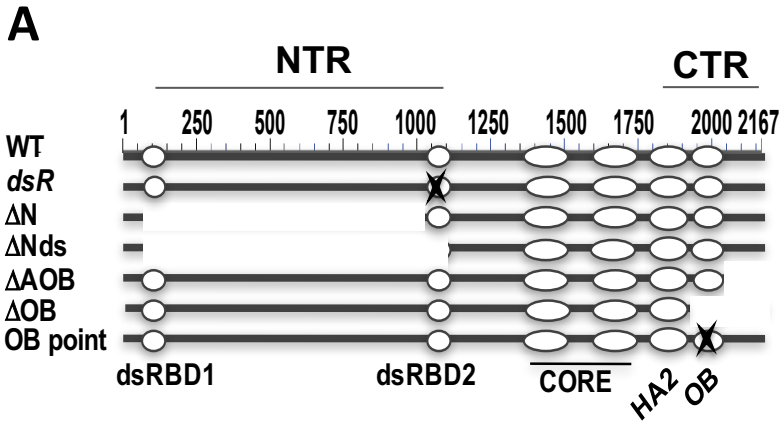

NAME	MUTATION	DOMAINS AFFECTED	MW
dsR	K1078A/A1086D	dsRBD2	242
ΔN	Δ34-1023	dsRBD1	132
ΔNds	Δ34-1093	dsRBD1/dsRBD2	124
ΔAOB	Δ1908-2167		228
ΔOB	Δ2045-2167	OB fold	213
1979	R1979A	OB fold	242
1998	H1998E	OB fold	242
1999	R1999E	OB fold	242
98/99	H1998E/R1999E	OB fold	242
2023	R2023A	OB fold	242

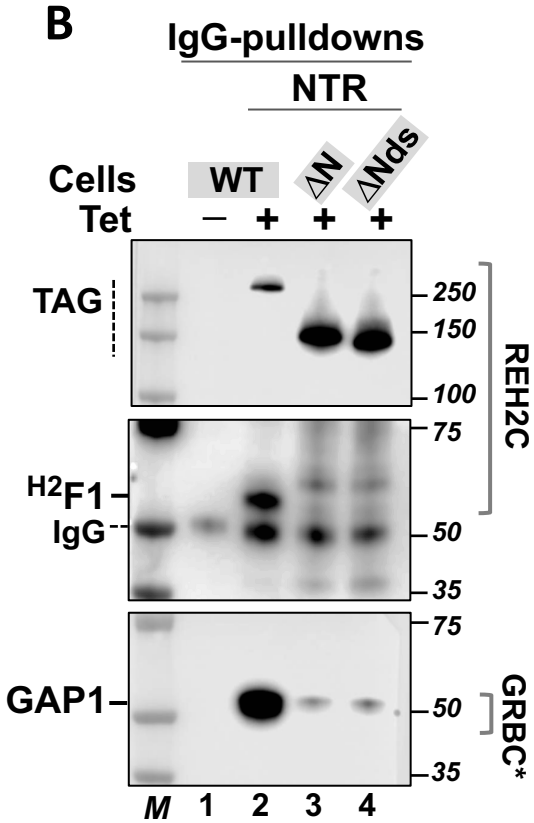

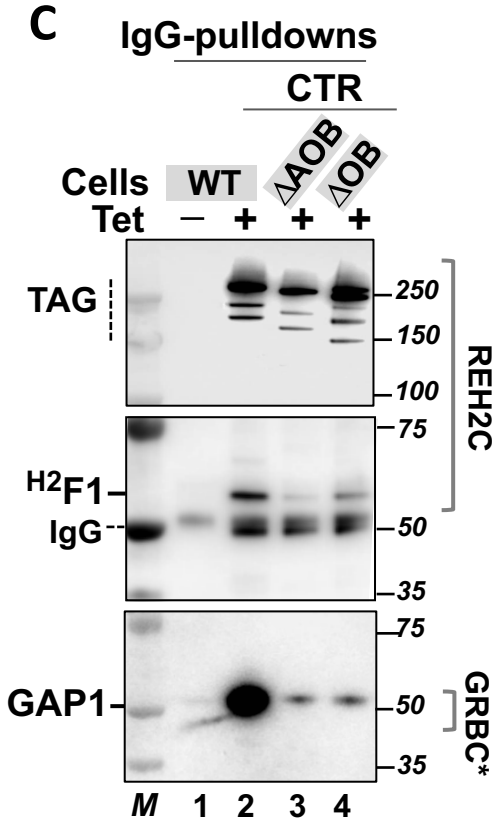

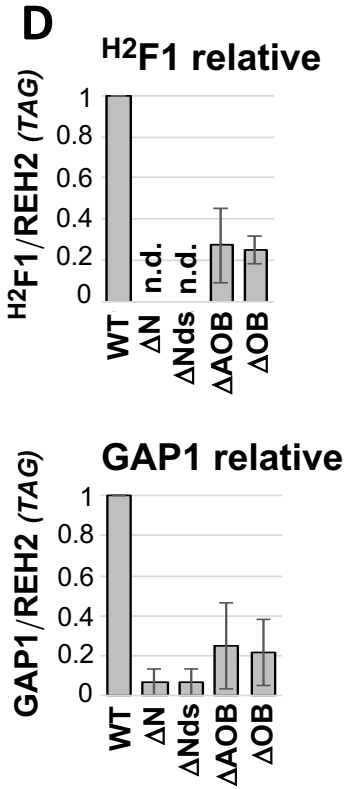

Figure 1

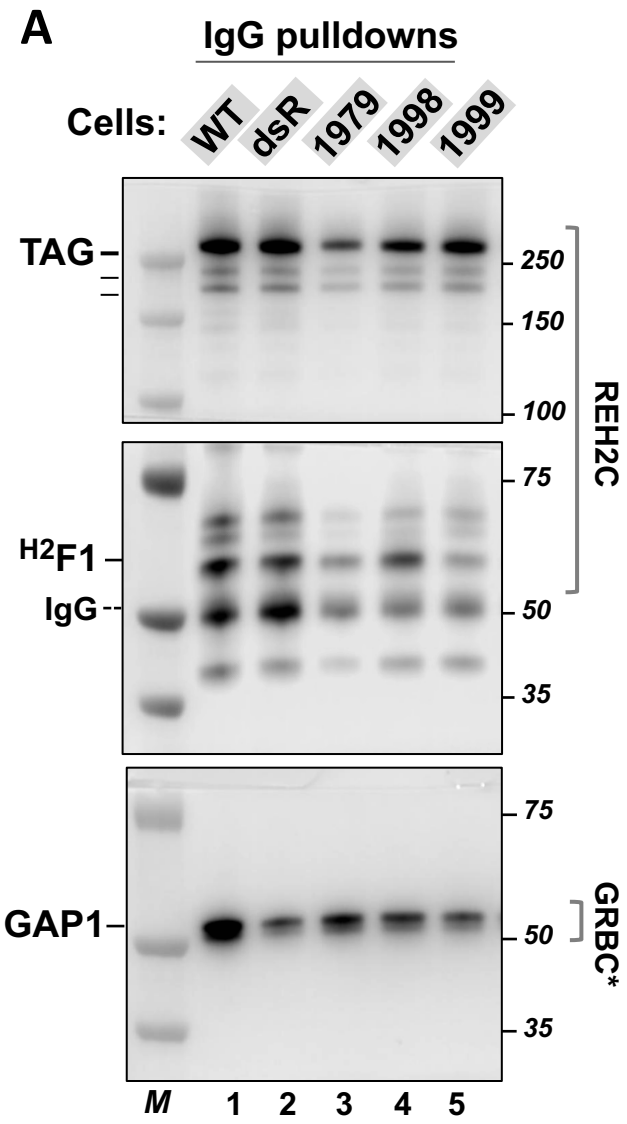
A
IgG pulldowns
Cells:
WT
dsR
1979
1998
1999
TAG
H2F1
IgG
GAP1
250
150
100
75
50
35
REH2C
GRBC*
M
1
2
3
4
5

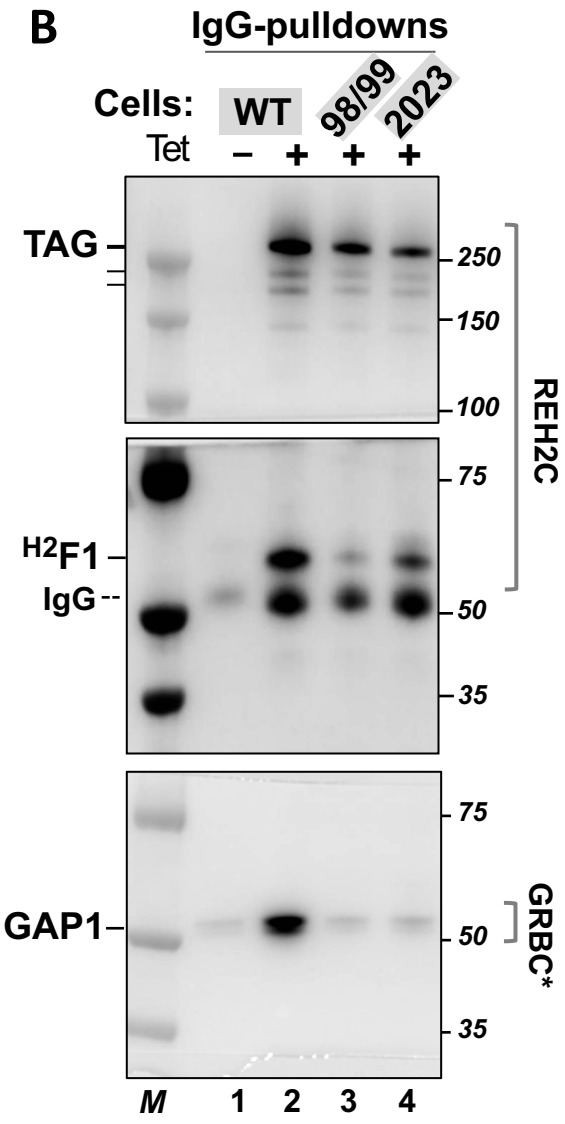
B
IgG-pulldowns
Cells:
WT
98/99
2023
Tet
–
+
+
+
TAG
H2F1
IgG
GAP1
250
150
100
75
50
35
REH2C
GRBC*
M
1
2
3
4

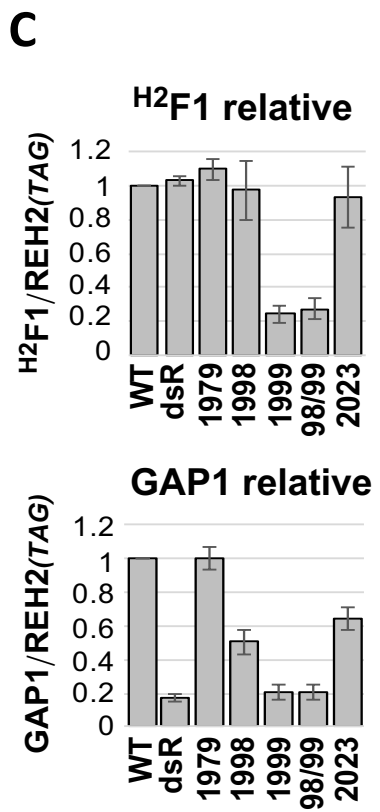
C
H2F1 relative
H2F1/REH2(TAG)
1.2
1
0.8
0.6
0.4
0.2
0
WT
dsR
1979
1998
1999
98/99
2023
GAP1 relative
GAP1/REH2(TAG)

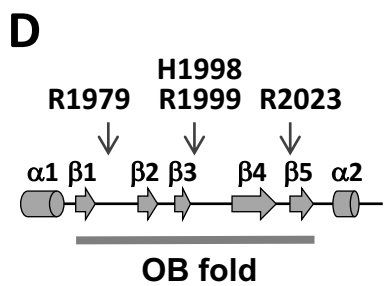
D
R1979
H1998
R1999
R2023
α1
β1
β2
β3
β4
β5
α2
OB fold

Figure 2

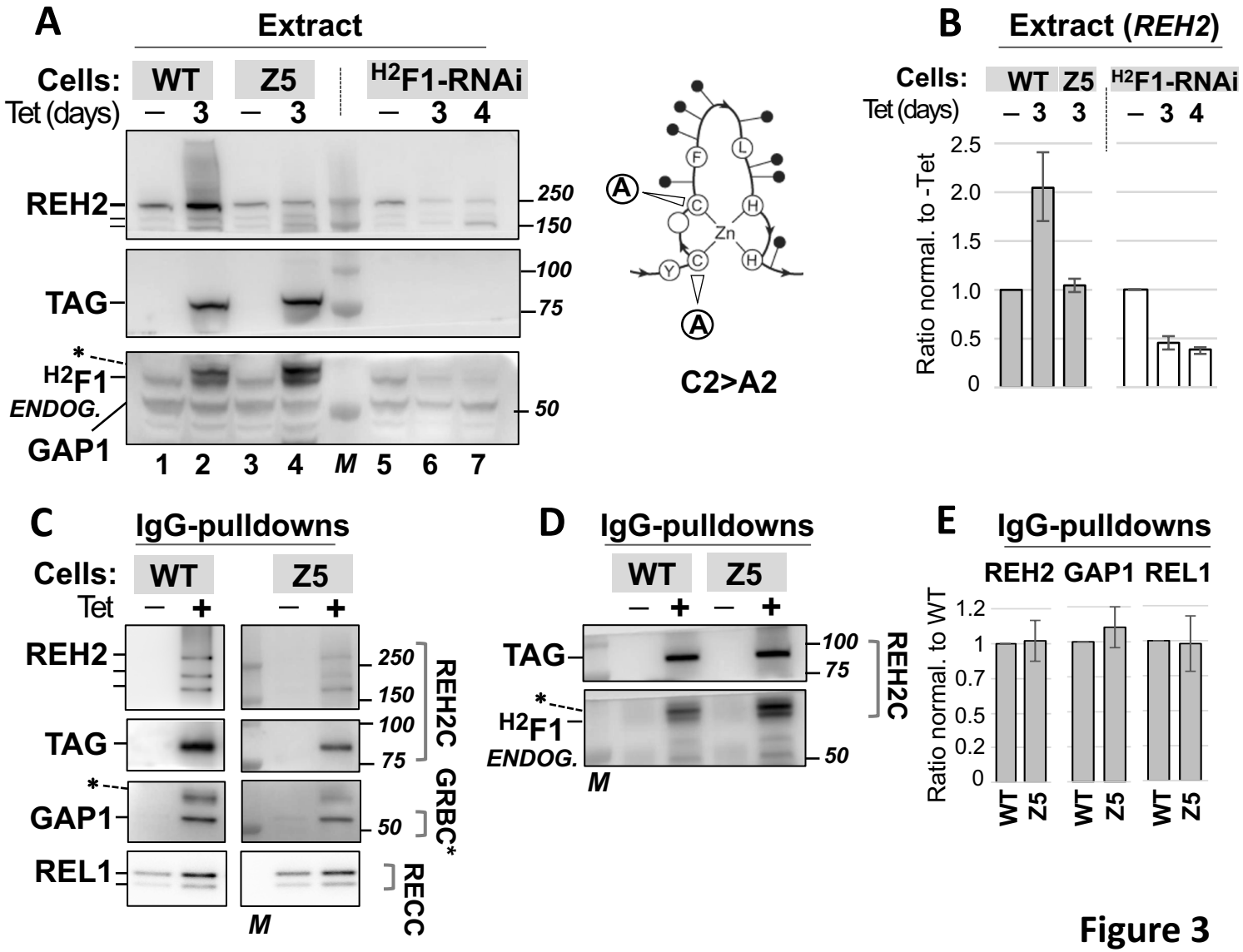
A
Extract
Cells: WT Z5 H2F1-RNAi
Tet (days) – 3 – 3 – 3 4
REH2
TAG
H2F1
ENDOG.
GAP1
250
150
100
75
50
1 2 3 4 M 5 6 7
C2>A2
B
Extract (REH2)
Cells: WT Z5 H2F1-RNAi
Tet (days) – 3 3 – 3 4
Ratio normal. to -Tet
2.5
2.0
1.5
1.0
0.5
0
C
IgG-pulldowns
Cells: WT Z5
Tet – + – +
REH2
TAG
GAP1
REL1
M
REH2C
GRBC*
RECC
D
IgG-pulldowns
WT Z5
– + – +
TAG
H2F1
ENDOG.
M
REH2C
E
IgG-pulldowns
REH2 GAP1 REL1
Ratio normal. to WT
1.2
1
0.7
0.5
0.2
0
WT Z5 WT Z5 WT Z5

Figure 3

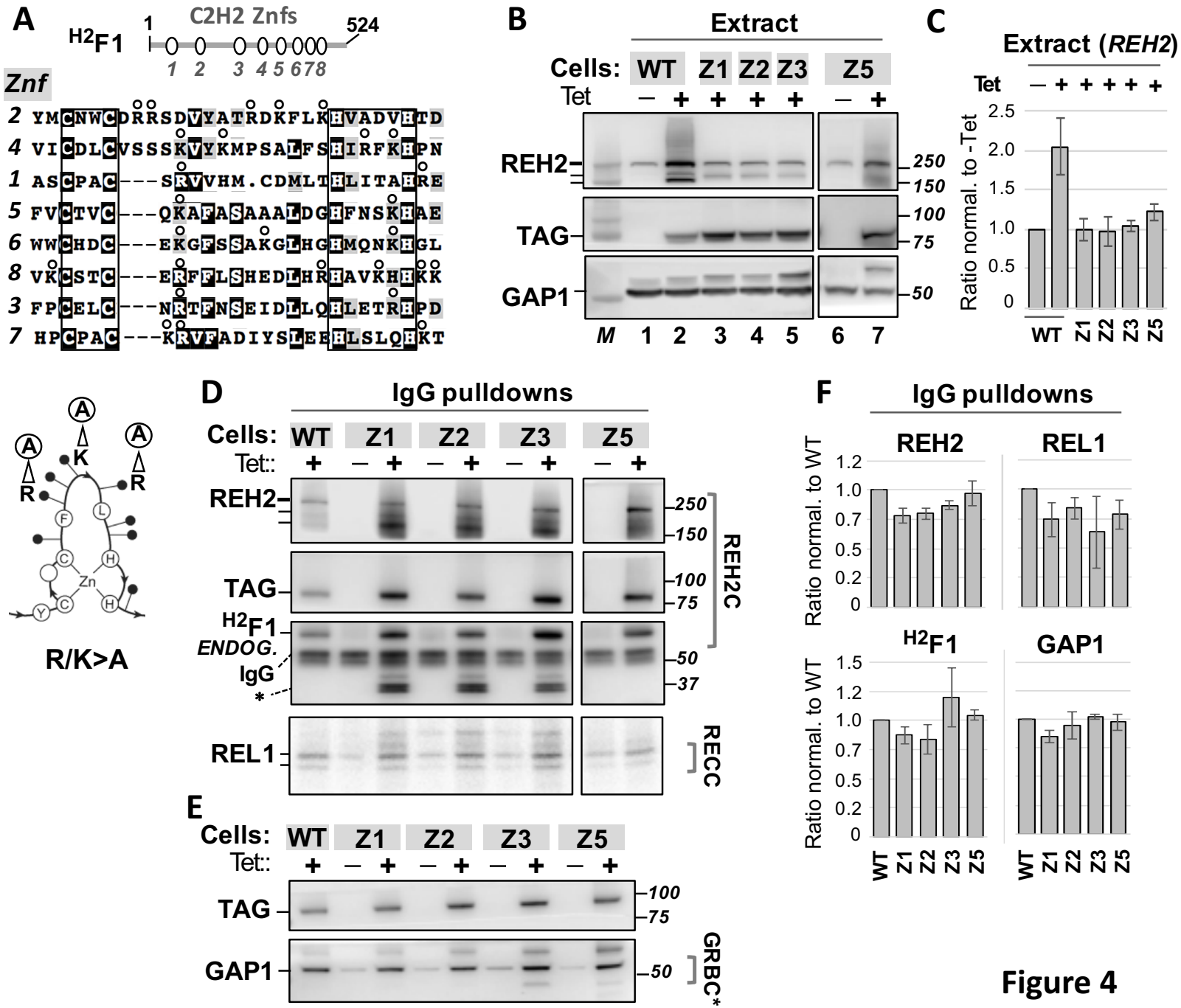
A
H2F1
C2H2 Znfs
1
524
1 2 3 4 5 6 7 8
Znf
2 YMCNWCDRRSDVYATRDKFLKHVADVHTD
4 VICDLCVSSSKVYKMPSALFSHIRFKHPN
1 ASCPAC---SRVVHM.CDMLTHLITAHRE
5 FVCTVC---QKAFASAAALDGHFNSKHAE
6 WWCHDC---EKGFSSAKGLHGHMQNKHGL
8 VKCSTC---ERFFLSHEDLHRHAVKHHKK
3 FPCELC---NRTFNSEIDLLQHLETRHPD
7 HPCPAC---KRVFADIYSLEEHLSLQHKT
B
Extract
Cells: WT Z1 Z2 Z3 Z5
Tet – + + + + – +
REH2
TAG
GAP1
250
150
100
75
50
M 1 2 3 4 5 6 7
C
Extract (REH2)
Tet – + + + + +
Ratio normal. to -Tet
2.5
2.0
1.5
1.0
0.5
0
WT Z1 Z2 Z3 Z5
A
K
R
R
F
L
C
H
Zn
Y
C
H
R/K>A
D
IgG pulldowns
Cells: WT Z1 Z2 Z3 Z5
Tet:: + – + – + – + – +
REH2
TAG
H2F1
ENDOG.
IgG
*
REL1
250
150
100
75
50
37
REH2C
RECC
E
Cells: WT Z1 Z2 Z3 Z5
Tet:: + – + – + – + – +
TAG
GAP1
100
75
50
GRBC*
F
IgG pulldowns
REH2
REL1
H2F1
GAP1
Ratio normal. to WT
1.2
1.0
0.7
0.5
0.2
0
1.5
WT Z1 Z2 Z3 Z5

Figure 4

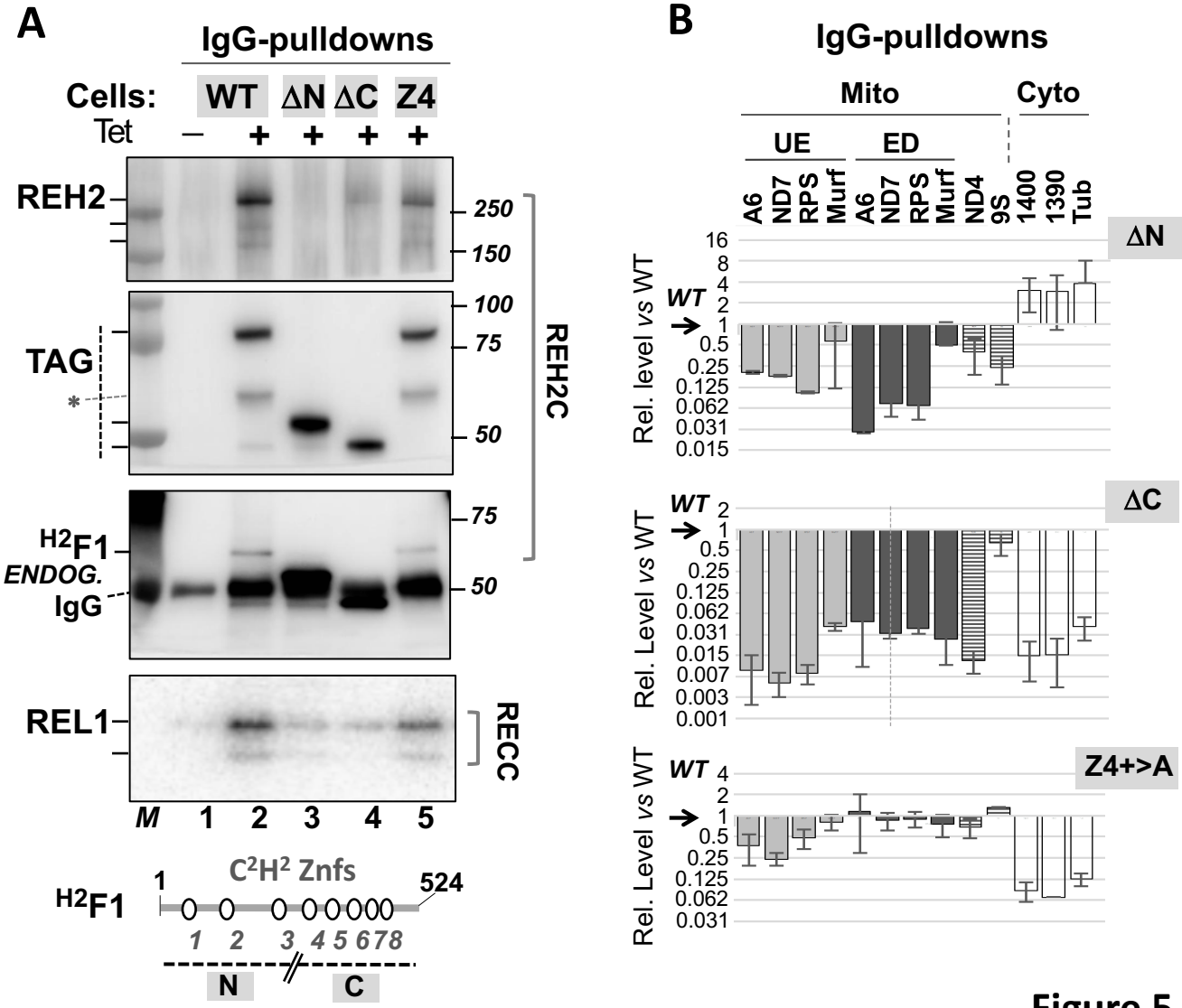
A
IgG-pulldowns
Cells:
WT
ΔN
ΔC
Z4
Tet
REH2
TAG
H2F1
ENDOG.
IgG
REL1
250
150
100
75
50
REH2C
RECC
M
1
2
3
4
5
C2H2 Znfs
524
N
C
B
Mito
Cyto
UE
ED
A6
ND7
RPS
Murf
ND4
9S
1400
1390
Tub
Rel. level vs WT
Rel. Level vs WT
WT
Z4+>A

Figure 5

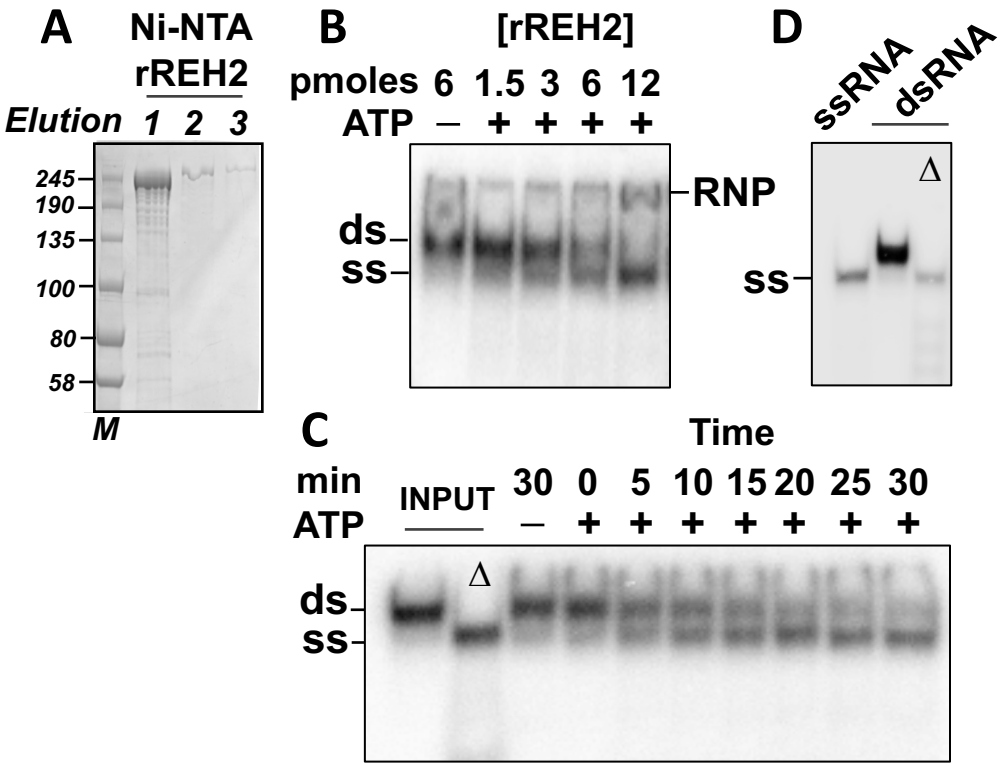
A
Ni-NTA
rREH2
Elution 1 2 3
245
190
135
100
80
58
M
B
[rREH2]
pmoles 6 1.5 3 6 12
ATP – + + + +
RNP
ds
ss
D
ssRNA
dsRNA
Δ
ss
C
Time
min
INPUT 30 0 5 10 15 20 25 30
ATP – + + + + + + +
Δ
ds
ss

Figure 6